

Building a More Predictive Protein Force Field: A Systematic and Reproducible Route to AMBER-FB15

Lee-Ping Wang, Keri A. McKiernan, Joseph Gomes, Kyle A. Beauchamp, Teresa Head-Gordon, Julia E. Rice, William C. Swope, Todd J. Martínez, and Vijay S. Pande

J. Phys. Chem. B, **Just Accepted Manuscript** • DOI: 10.1021/acs.jpcc.7b02320 • Publication Date (Web): 17 Mar 2017

Downloaded from <http://pubs.acs.org> on April 1, 2017

Just Accepted

“Just Accepted” manuscripts have been peer-reviewed and accepted for publication. They are posted online prior to technical editing, formatting for publication and author proofing. The American Chemical Society provides “Just Accepted” as a free service to the research community to expedite the dissemination of scientific material as soon as possible after acceptance. “Just Accepted” manuscripts appear in full in PDF format accompanied by an HTML abstract. “Just Accepted” manuscripts have been fully peer reviewed, but should not be considered the official version of record. They are accessible to all readers and citable by the Digital Object Identifier (DOI®). “Just Accepted” is an optional service offered to authors. Therefore, the “Just Accepted” Web site may not include all articles that will be published in the journal. After a manuscript is technically edited and formatted, it will be removed from the “Just Accepted” Web site and published as an ASAP article. Note that technical editing may introduce minor changes to the manuscript text and/or graphics which could affect content, and all legal disclaimers and ethical guidelines that apply to the journal pertain. ACS cannot be held responsible for errors or consequences arising from the use of information contained in these “Just Accepted” manuscripts.



Building a More Predictive Protein Force Field: A Systematic and Reproducible Route to AMBER-FB15

Lee-Ping Wang, Keri A. McKiernan, Joseph Gomes, Kyle A. Beauchamp, Teresa Head-Gordon, Julia E. Rice, William C. Swope, Todd J. Martínez, and Vijay S. Pande*

ABSTRACT

The increasing availability of high-quality experimental data and first-principles calculations creates opportunities for developing more accurate empirical force fields for simulation of proteins. We developed the AMBER-FB15 protein force field by building a high-quality quantum chemical data set consisting of comprehensive potential energy scans and employing the ForceBalance software package for parameter optimization. The optimized potential surface allows for more significant thermodynamic fluctuations away from local minima. In validation studies where simulation results are compared to experimental measurements, AMBER-FB15 in combination with the updated TIP3P-FB water model predicts equilibrium properties with equivalent accuracy, and temperature dependent properties with significantly improved accuracy, in comparison with published models. We also discuss the effect of changing the protein force field and water model on the simulation results.

INTRODUCTION

Molecular Dynamics (MD) simulations have demonstrated high utility for the functional study of biomolecular systems. The degree of spatial and temporal resolution afforded by this technique allows for atomic-scale analysis of structure, dynamics, and function. In order to achieve time scales relevant to biological processes, a classical interaction potential, or force field, is typically used. Although approximate, these models are a vital part of developing the mechanistic, thermodynamic, and kinetic understanding of biological phenomena including but

* Email: pande@stanford.edu

1
2
3 not limited to enzyme catalysis¹⁻¹⁰, protein folding¹¹⁻¹⁸, protein-ligand binding,¹⁹⁻²⁶ and protein
4
5 conformational change.²⁷⁻³³ The results of these studies strongly depend on the accuracy of the
6
7 underlying force field. While there have been noteworthy simulations on protein dynamics using
8
9 a quantum chemical potential energy surface,³⁴⁻³⁶ these are still incapable of realizing dynamics
10
11 on the biologically relevant timescales (ns and beyond) for larger proteins (200 residues and
12
13 beyond). Therefore, the development of accurate empirical force fields is still crucial for
14
15 computational biomolecular simulation.
16
17
18

19
20 The conceptual development of the consistent force field is credited to Lifson who proposed
21
22 that the interactions between atoms could be described using an energy function and a small set
23
24 of transferable empirical parameters. In 1967, Lifson, Warshel and Levitt successfully derived
25
26 and parameterized the first force field.³⁷ In 1969, this idea was implemented by Levitt with the
27
28 first computer simulation of a protein.³⁸
29
30

31
32 Important to the future of condensed phase force fields was the development of the
33
34 Optimized Potentials for Liquid Simulations (OPLS) model proposed by Jorgenson in the
35
36 1980s.³⁹ Here the nonbonded interactions were derived by fitting to experimental thermodynamic
37
38 properties of organic liquids, a method which inspired parameterization methodologies of the
39
40 first generation of all-atom protein force fields. The CHARMM force field was also introduced
41
42 in the 1980s along with the molecular dynamics program of the same name,⁴⁰ and the force field
43
44 has undergone several significant revisions in recent years as experimental and ab initio data
45
46 have improved.⁴¹⁻⁴³ As subsequent developments are too numerous to describe here, we refer the
47
48 reader to some more comprehensive reviews.⁴⁴⁻⁴⁷
49
50
51

52
53 One of the first force fields capable of all-atom simulations of proteins in water is of the
54
55 AMBER type and referred to as ff94.⁴⁸ This model approximates the energy of a system of
56
57
58
59
60

1
2
3 molecules as a sum of terms including harmonic bonds, harmonic angles, electrostatic
4 interactions, Lennard-Jones repulsion and dispersion interactions, and dihedral energy terms for
5 adjusting the energy profiles of bond rotations. Harmonic bond and angle terms were optimized
6 to reproduce experimental normal mode frequencies by fitting to structural and vibrational
7 frequency data on small molecule fragments of amino and nucleic acids. The atom-centered
8 point charges were fit using Kollman's RESP method, which aims to reproduce the electrostatic
9 potential of a target molecule to calculations at the HF/6-31G* quantum level of theory;⁴⁹ this
10 process was accelerated significantly using Bayly's semiempirical AM1-BCC approach.⁵⁰⁻⁵¹ The
11 Lennard-Jones parameters were fit in order to reproduce densities and enthalpies of vaporization
12 in simulations of organic liquids (as was done for OPLS). The dihedral parameters were fit using
13 relative energies of alanine and glycine dipeptide conformers calculated via quantum mechanical
14 (QM) methods at the MP2/6-31G* level.

15
16
17
18
19
20
21
22
23
24
25
26
27
28
29
30
31
32
33
34
35
36
37
38
39
40
41
42
43
44
45
46
47
48
49
50
51
52
53
54
55
56
57
58
59
60
The subsequent widely adopted major iterations of the AMBER type force field have carried
over the functional form and most parameters from the original ff94 model. These more recent
developments focused primarily on improving protein secondary structure representation via the
successive refitting of the ff94 dihedral parameters. The torsions in ff94 applied equally to all
quartets of atoms around a bond between two atom types; the parameters were fit to a set of
experimental small molecule barrier heights. The ff99 force field⁵² improved upon this approach
by introducing explicit four atom dihedral terms that were fit to a larger set of small molecules,
as well as a reference set of alanine tetrapeptide conformers. The ff99SB force field⁵³ was
introduced by Hornak and Simmerling to improve conformational preferences for glycine and
address known deficiencies of previous AMBER force fields such as over-stabilization of α -
helices.⁵⁴ The amino acid backbone dihedrals for glycine and alanine were refit using a grid-

1
2
3 based conformational scan of alanine and glycine tetrapeptides. In ff99 and ff99SB, the other
4 protein parameter types were left unmodified from ff94. The ff99SB-ILDN⁵⁵ force field of Shaw
5 and coworkers introduced explicit side chain parameters for four specific residue types
6 (isoleucine, leucine, aspartate, and asparagine). The explicit side chain parameters were fit to
7 grid-based conformational scans calculated using second-order Møller-Plesset perturbation
8 theory with the resolution of the identity approximation⁵⁶⁻⁵⁷ (RI-MP2) and a correlation-
9 consistent augmented triple zeta basis set⁵⁸ (aug-cc-pVTZ), and validated by calculating NMR
10 observables from simulation trajectories and comparing to experiment. The ff99SB-NMR force
11 field of Li and Bruschweiler was explicitly fit to NMR data by matching chemical shift
12 predictions from MD trajectories to experiment.⁵⁹ Although each successive modifications of the
13 ff99 force field led to further improvements in secondary structure, the temperature dependence
14 of partial folding remained a major limitation for these models.⁶⁰

15
16
17
18
19
20
21
22
23
24
25
26
27
28
29
30
31
32 Today, researchers are looking in the directions of replacing the point charge model carried
33 over from ff94 with new fixed-charge models and non-additive electrostatic potentials that
34 include explicit polarization. The implicitly polarized charge model⁶¹ found in the ff15ipq⁶² force
35 fields treats the point charges of a target molecule as a sum of the charges calculated in vacuum
36 and a perturbation of these charges caused by the presence of explicit solvent molecules, and in
37 this way accounts for electrostatic polarization in a nonpolarizable model. The addition of
38 polarizability in the form of Drude particles⁶³ or induced dipoles⁶⁴ produces a more physically
39 realistic model of electrostatic polarization; however, these models incur a significantly greater
40 computational cost which limits the timescales that are accessible compared with fixed-charge
41 models. These new electrostatic models show great promise for improving the accuracy of the
42 protein energy potential. However, protein force fields that incorporate these electrostatic models
43
44
45
46
47
48
49
50
51
52
53
54
55
56
57
58
59
60

1
2
3 require refitting of the other bonded and nonbonded parameter types, and they have yet to be
4
5 tested to the same extent as the RESP model. It is likely that fine-tuning of bonded and van der
6
7
8
9
10
11
12
13
14
15
16
17
18
19
20
21
22
23
24
25
26
27
28
29
30
31
32
33
34
35
36
37
38
39
40
41
42
43
44
45
46
47
48
49
50
51
52
53
54
55
56
57
58
59
60

require refitting of the other bonded and nonbonded parameter types, and they have yet to be tested to the same extent as the RESP model. It is likely that fine-tuning of bonded and van der Waals interactions using high quality *ab initio* data will continue to be an essential part of developing future generations of protein force fields.

In this work our goal is to assess the limits of accuracy that can be attained by fitting intramolecular bond, angle, and dihedral parameters to QM calculations without modifying the functional form and nonbonded parameters, which we expect will complement efforts currently being undertaken to improve the nonbonded part. We systematically explore the modification of bond, angle, and dihedral parameters, taking the ff99SB functional form and parameter set as a starting point. We introduce a new potential energy scanning method to build an improved data set of dipeptide conformations and provide unprecedented coverage of the conformational space. The parameter optimization was done using ForceBalance,⁶⁵ an open-source software package designed to enable reproducible and systematic force field development.

The new parameter set is validated by calculating thermodynamic observables from protein simulations and comparing to experiment. We find that the new parameter set performs equally well as the previous models for equilibrium properties, where previous models gave good agreement with experiment, and gives superior performance for temperature dependence, where previous models perform poorly. Our main finding from the parameter re-optimization is that the ff99SB, and related similarly derived models, overestimate the steepness of potential energy basins, which explains why they predict the correct equilibrium structures, but may lead to problems when simulating conformational changes or deviations from these structures as observed in our subsequent validation studies.

1
2
3 Our validation testing includes a comparison of protein force fields combined with four water
4 models: the TIP3P model most widely used in protein simulations, the updated and more
5 accurate TIP3P-FB model⁶⁵, and the four-point TIP4P-Ew⁶⁶ and TIP4P-FB⁶⁵ models. TIP4P-Ew
6 is a four-point water model developed for use with the particle mesh Ewald electrostatics
7 method⁶⁷ that is ubiquitous today, and was among the first water models parameterized to
8 accurately reproduce the temperature dependence of the density.⁶⁶ The TIP3P-FB and TIP4P-FB
9 models, developed ten years later, use the same functional form as TIP3P and TIP4P-Ew
10 (respectively) and were systematically parameterized to reproduce the temperature and pressure
11 dependence of a wide range of thermodynamic properties.⁶⁵ Despite the advances made in water
12 models over the last two decades, the protein force fields have largely followed historical
13 precedent in that they are developed and tested for use with the TIP3P model, which raises
14 interesting questions of how the simulation accuracy may be affected if the water model is
15 changed. Here, our validation studies show that different force field / water model combinations
16 produce widely varying temperature dependence properties of the protein, and combining
17 AMBER-FB15 with TIP3P-FB produces the best agreement with experiment, despite the fact
18 that the protein intermolecular parameters were not optimized. We discuss some interesting
19 patterns in how different water models affect protein stability. We also describe common
20 limitations of all tested models, which include underestimation of the slopes of protein melting
21 curves and overly collapsed denatured state ensembles, highlighting the necessity of improved
22 descriptions of nonbonded interactions.
23
24
25
26
27
28
29
30
31
32
33
34
35
36
37
38
39
40
41
42
43
44
45
46
47
48
49

50 The force field combination AMBER-FB15/TIP3P-FB is recommended for general-purpose
51 simulations of proteins, particularly in situations where fluctuations away from equilibrium and
52 temperature dependence are expected to play an important role. Additionally, the *ab initio* data
53
54
55
56
57
58
59
60

set used to parameterize AMBER-FB15 has been made publicly available online,⁶⁸ and we expect it to be useful for force field development efforts in the community.

THEORY

AMBER functional form. The AMBER99SB protein force field (abbreviated as A99SB) is the starting point of the parameterization in this work; it consists of the simple and well-known functional form put forth in AMBER94 (here referred to as the AMBER functional form), the AMBER99 parameter set, and the “SB” correction to the protein backbone dihedral parameters.⁵³ In the AMBER functional form, the total potential energy of the system is written as a sum of bonded and nonbonded contributions:

$$\begin{aligned}
 E &= E_{\text{bond}} + E_{\text{angle}} + E_{\text{dihedral}} + E_{\text{improper}} + E_{\text{vdW}} + E_{\text{ele}}, \\
 E_{\text{bond}} &= \sum_{i,j \in \text{bonds}} \frac{k_{ij}^b}{2} (r_{ij} - r_{ij}^0)^2, \quad E_{\text{angle}} = \sum_{i,j,k \in \text{angles}} \frac{k_{ijk}^\theta}{2} (\theta_{ijk} - \theta_{ijk}^0)^2, \\
 E_{\text{dihedral}} &= \sum_{i,j,k,l \in \text{dihedrals}} \sum_{n=1}^6 k_{ijkl,n}^\phi (1 + \cos(n\phi_{ijkl} - \phi_{ijkl,n}^0)), \\
 E_{\text{improper}} &= \sum_{i,j,k,l \in \text{impropers}} k_{ijkl,2}^\phi (1 + \cos(2\phi_{ijkl})), \\
 E_{\text{vdW}} &= \sum_{i,j \in \text{nonbonded}} 4\epsilon_{ij} \left[-\left(\frac{\sigma_{ij}}{r_{ij}}\right)^6 + \left(\frac{\sigma_{ij}}{r_{ij}}\right)^{12} \right] \\
 E_{\text{ele}} &= \sum_{i,j \in \text{nonbonded}} \frac{q_i q_j}{r_{ij}},
 \end{aligned} \tag{1}$$

where i, j, k, l are atomic indices and $r_{ij}, \theta_{ijk}, \phi_{ijkl}$ are functions of the atomic coordinates. The empirical parameters for bonded interactions are denoted as $k_{ij}^b, r_{ij}^0, k_{ijk}^\theta, \theta_{ijk}^0, k_{ijkl,n}^\phi, \phi_{ijkl,n}^0$ and depend on the *atom types* of the atoms involved. This work focuses on optimizing the bonded parameters, in some cases defining new atom types to increase the size of the parameter space.

In the nonbonded interactions involving pairs of atoms separated by 3 or more bonds, the pairwise Lennard-Jones parameters σ_{ij} and ϵ_{ij} are derived from those of individual atom types (σ_i and ϵ_i) via the Lorentz-Berthelot combining rules, and the atomic partial charges q_i are defined for each atom in each amino acid. These parameters are not modified in this work. The vdW and electrostatic interactions between pairs of atoms separated by exactly three bonds (i.e. “1-4 pairs”) are reduced by factors of 1.2 and 2.0, respectively; the 1-4 interactions are nominally considered to be a kind of bonded interaction, but they are also not modified in this work.

Reference Data	# Calcs.
Energy, gradients of 26 amino acids over (φ , ψ) (incl. ASH, CYM, GLH, HIE, HIP, LYN)	14,971
Energy, gradients of 21 amino acids over (χ_1 , χ_2) (excluding ALA, CYM, GLY, PRO, VAL)	12,093
Energy, gradients of CYM, VAL over (φ , χ_1)	1,151
Vibrational frequencies and eigenvectors for 20 amino acids	20
Energy, gradients of MM-optimized structures	1,060

Table 1. Types of parameterization data for AMBER-FB15 force field.

Reference data set. We constructed a database of *ab initio* calculations, summarized in Table 1, consisting of single-point energies, nuclear gradients, and vibrational modes calculated for the blocked dipeptides ACE-X-NME containing one amino acid side chain. This database is further supplemented by additional single-point energies and gradients evaluated at optimized geometries using intermediate force field parameter sets, described later. All energy and gradient values in the database were respectively computed at the RI-MP2/CBS and RI-MP2/aug-cc-pVTZ levels of theory; the calculations were performed in the gas phase. For each dipeptide, a 24x24 grid of structures was generated by constraining the backbone dihedral angles φ and ψ at 15-degree increments and minimizing the energy in the orthogonal degrees of freedom; a second

1
2
3 grid for the side chain dihedral angles χ_1 and χ_2 was carried out for all amino acids with a side
4
5 chain, except for valine and deprotonated cysteine (CYM) where the second grid uses φ and χ_1
6
7 instead.
8
9

10 Beyond the simplest dipeptides (i.e. glycine and alanine), the potential energy surfaces
11
12 contain many local minima that cannot be comprehensively searched using local optimization
13
14 methods. Moreover, a sequence of constrained geometry optimizations through a full rotation of
15
16 a dihedral angle may not return to the starting structure, analogous to turning a corkscrew
17
18 embedded in a cork. This hysteresis is a consequence of the many orthogonal degrees of freedom
19
20 that are only locally optimized using the previous structure as the initial guess. Our approach for
21
22 scanning the potential surface attempts to find the lowest-energy local minimum in the
23
24 orthogonal degrees of freedom, as they are likely to carry a higher thermodynamic weight in the
25
26 protein. To this end we developed the following procedure to explore the conformational space
27
28 using lower levels of theory:
29
30
31
32

- 33
34 1. Obtain a four-dimensional grid of structures using gas-phase simulated annealing simulations
35
36 and the AMOEBA13 polarizable force field; the number of grid points was 12, 12, 6, 6 for φ ,
37
38 ψ , χ_1 and χ_2 respectively, giving a total of 5184 points for each amino acid.
39
40
- 41 2. For each structure on the four-dimensional grid, perform a MP2/6-31+G* geometry
42
43 optimization with φ , ψ , χ_1 and χ_2 constrained.
44
45
- 46 3. For two chosen dihedral angles (e.g. φ , ψ), map the four-dimensional grid of structures to the
47
48 two-dimensional grid and record the structure with the lowest energy, denoted by $q_{\varphi,\psi}, E_{\varphi,\psi}$.
49
50 Note that after step 2, only one structure for each (φ, ψ) grid point is recorded out of a total
51
52 of 36.
53
54
55
56
57
58
59
60

1
2
3 4. For each 2-D grid point (φ , ψ) containing a new lowest energy structure, initialize four
4
5
6

7
8 MP2/6-31+G* geometry optimizations with new dihedral angle constraints $\varphi \pm \frac{\pi}{12}, \psi \pm \frac{\pi}{12}$.
9

10 5. Repeat steps 3 and 4 until no new lowest-energy structures are found. The end result is a
11
12

13
14 $\frac{\pi}{12}$
15 24x24 grid of structures with a resolution of $\frac{\pi}{12}$.
16

17 In each iteration of steps 3 and 4, each grid point with a new lowest-energy structure is used to
18
19 launch four new geometry optimizations at the neighboring grid points, and the procedure is
20
21 carried out recursively until no more lowest-energy structures are found. The number of times
22
23 the recursive procedure was iterated depended on the side chain flexibility of the amino acid,
24
25 ranging from 6 (ALA, GLY) to 24 (GLU). At the conclusion of the calculation, each structure is
26
27 minimized over the initial configurations of its four neighboring structures, and this condition is
28
29 satisfied for the entire surface; the result is a grid of structures where the energy changes by as
30
31 little as possible between the grid points, although the geometry may change significantly along
32
33 the orthogonal degrees of freedom. Following this, each structure is re-optimized at the RI-
34
35 MP2/aug-cc-pVDZ level with the same dihedral constraints. A single RI-MP2/aug-cc-pVQZ
36
37 calculation at the optimized geometry provides the means to estimate the energy in the MP2/CBS
38
39 limit using Helgaker's two-point extrapolation.⁶⁹ The gradient computed at the RI-MP2/aug-cc-
40
41 pVTZ level is also added to this data set.
42
43
44
45
46

47 We also carried out a geometry optimization and frequency calculation at the RI-MP2/aug-
48
49 cc-pVTZ level for the overall lowest-energy structure and scaled the frequencies using standard
50
51 scaling factors.⁷⁰ Two separate scaling factors were used – 0.960 for high frequencies and 1.012
52
53 for low frequencies, using 1000 cm⁻¹ to distinguish the high-frequency and low-frequency
54
55 regions.
56
57
58
59
60

In frequency regions near the dividing line, using these multiplicative scaling factors could cause vibrational frequencies to switch order. To prevent this from happening, the frequency shifts Δ_h for vibrations ν_h above 1000 cm^{-1} are attenuated with the following formula:

$$\Delta_h = \Delta_{h,0} s_h, \text{ where } \Delta_{h,0} = (0.96 - 1.0)\nu_h, \text{ and } s_h = \frac{\nu_h - \nu_d}{\nu_h - 0.96\nu_d}. \quad (2)$$

When ν_h approaches the dividing frequency $\nu_d = 1000\text{ cm}^{-1}$, the attenuating factor ensures that the scaled frequency never falls below the dividing frequency. A similar attenuating factor is defined for vibrational frequencies ν_l below 1000 cm^{-1} :

$$\Delta_l = \Delta_{l,0} s_l \text{ where } \Delta_{l,0} = (1.012 - 1.0)\nu_l, \text{ and } s_l = \frac{\nu_l - \nu_d}{\nu_l - 1.012\nu_d}. \quad (3)$$

Parameter optimization. The parameters were optimized using the ForceBalance software package.^{65, 71-72} ForceBalance provides a framework where the differences between force field predictions and provided reference data are used to construct a weighted least-squares objective function and its derivatives. A regularization term (penalty function) is applied to prevent large parameter deviations where reference data is insufficient or the force field contains linear dependencies. The calculation is fully specified by:

- (1) the functional form of the force field, parameter space (i.e. selection of which parameters to optimize and their interdependencies) and initial parameter values,
- (2) the *targets* and their weights that contribute to the objective function,
- (3) the *prior widths* that constrain the parameter deviations from their initial values, and
- (4) the optimization algorithm that minimizes the objective function.

A major advantage of using ForceBalance is that the calculation is precisely specified and systematically carried out, ensuring that the results are reproducible and significantly reducing the effort involved when repeating the calculation with any component added or changed.

We used the functional form and initial parameters from the AMBER99SB force field; the choice of parameter space was decided by exploring the possible combinations of options in tuning the bond, angle, and torsional parameters, as described in the results and discussion section. We also explored defining independent dihedral parameters for amino acid side chains, which goes beyond the flexibility of the original AMBER99SB model. The extension of AMBER using side chain specific parameters has previously been explored in models such as AMBER99SB-ILDN, RSFF2⁷³ and AMBER14SB.⁷⁴

The objective function is defined as a function of the differences between the force field predictions and the reference data, plus a regularization term that penalizes large parameter deviations from the initial values. The three types of targets and penalty term are combined as:

$$\chi^2 = \sum_{i=1}^{N_{\text{grids}}} \chi_{\text{grid};i}^2 + \sum_{i=1}^{N_{\text{AA}}} \chi_{\text{vib};i}^2 + 4 \sum_{i=1}^{N'_{\text{AA}}} \chi_{\text{MM}_{\text{opt}};i}^2 + \sum_{i=1}^{N_{\text{prm}}} \left(\frac{\alpha_i - \alpha_i^0}{p_i} \right)^2. \quad (4)$$

The first term χ_{grid}^2 represents the contributions from the energies and gradients evaluated over a two-dimensional dihedral grid:

$$\chi_{\text{grid}}^2 = \left\langle w_E \frac{(E_{MM} - E_{QM})^2}{\langle E_{QM}^2 \rangle - \langle E_{QM} \rangle^2} + \frac{w_F |F_{MM} - F_{QM}|^2}{3N_{\text{atom}} \langle |F_{QM}|^2 \rangle} \right\rangle \quad (5)$$

where E_{MM}, F_{MM} and E_{QM}, F_{QM} represent the energies and forces determined using the MM force field and QM reference set, respectively. The MM and QM energies are both referenced to the

structure with the lowest QM energy. Similarly, $w_E = 1.0$ and $w_F = 0.1$ are weighting factors for the energy and force error terms. The angle brackets denote a weighted average over the points, and the denominators ensure that the objective function has no physical units and the quantities are expressed as relative errors. The weighted average is given as:

$$\langle X \rangle \equiv \frac{\sum_{i=1}^{N_{pts}} w(E_{i,QM}) A(E_{i,MM} - E_{i,QM}) X_i}{\sum_{i=1}^{N_{pts}} w(E_{i,QM}) A(E_{i,MM} - E_{i,QM})}, \quad (6)$$

where the factors $w(E)$ and $A(E_{MM} - E_{QM})$ are given by:

$$w(E) = \begin{cases} D^{-1}, E \leq D \\ \left(D^2 + (E - D)^2 \right)^{-\frac{1}{2}}, E > D \\ 0, E > U \end{cases}; \quad A(\Delta) = \begin{cases} 1, \Delta \geq 0 \\ 100, \Delta < 0 \end{cases} \quad (7)$$

$w(E)$ is a decreasing function of the reference energy above the minimum, plotted in Figure 1.

$D = 5$ kcal/mol is the energy threshold below which $w(E)$ is a constant; above the threshold,

$w(E)$ becomes inversely proportional to the reference energy. $U = 20$ kcal/mol is the upper

energy cutoff above which the weight is set to zero. $A(E_{MM} - E_{QM})$ depends on the sign of the

MM-QM energy difference and heavily penalizes MM energies that are lower than the QM

energies. This reflects our experience that the positive and negative errors in the fit result in

asymmetric effects on the simulations. Configurations with negative $E_{MM} - E_{QM}$ have a

spuriously large thermodynamic weight and are more likely to appear during MM sampling,

which could shift the peaks of the distribution and lead to severe errors such as incorrect

1
2
3
4 equilibrium structures. On the other hand, configurations with positive $E_{MM} - E_{QM}$ have a
5
6 spuriously small weight in the MM ensemble and underestimate portions of the distribution; this
7
8 could result in overestimation of barriers and underestimation of fluctuations, which are (in a
9
10 sense) higher-order errors than incorrect equilibrium averages. Thus, enforcing $E_{MM} - E_{QM}$ to be
11
12 nonnegative everywhere and using a weight function that decays with E_{QM} forces the fitting
13
14 errors into the high-energy regions, where we expect the impacts on the thermodynamic
15
16 properties to be the smallest.
17
18
19
20

21
22 The second term χ_{vib}^2 represents the contributions from the vibrational frequencies evaluated
23
24 over the 20 standard amino acids:
25
26

$$\chi_{\text{vib}}^2 = \frac{1}{N_{\text{modes}}} \sum_{i=1}^{N_{\text{modes}}} \left(\frac{v_{i,MM} - v_{i,QM}}{100 \text{ cm}^{-1}} \right)^2 \quad (8)$$

27
28 The QM vibrational modes are ordered by increasing frequency, whereas the corresponding MM
29
30 vibrational mode is chosen to have the largest absolute value of the dot product with the QM
31
32 vibrational eigenvector. Unlike the energy and gradient calculations, the MM energy is
33
34 minimized prior to calculating the vibrational modes. Comparisons between eigencomponents
35
36 allows for relatively even weighting of high and low frequency modes. Although comparing the
37
38 force constant matrices would be more straightforward, it may overrepresent the higher
39
40 frequency modes that correspond to larger matrix elements.
41
42
43
44
45
46
47
48

49 The third term in the objective function addresses the appearance of spurious energy minima
50
51 in the MM force field in parts of configuration space not covered by the grid of structures. This
52
53 term consists of energies and gradients evaluated at MM-optimized structures as in Equation (6),
54
55 but without energy-dependent weights. We fully optimized each structure on the grid using the
56
57
58
59
60

MM force field without constraints and clustered the structures with a heavy-atom root-mean-square deviation (RMSD) cutoff of 0.1 Angstrom, leading to a small number of cluster centers for each amino acid (< 50). These structures were used to calculate MP2/CBS energies and MP2/aTZ gradients that were added to the objective function. Because updating the force field parameters changes the MM energy surface and the locations of minima, this cycle can be repeated to eliminate spurious minima that appear for the new parameter set.

Parameter Type	Prior Width
Bond length	0.01 nm
Bond force constant	$10^5 \text{ kJ mol}^{-1} \text{ nm}^{-2}$
Bond angle	5°
Angle force constant	$100 \text{ kJ mol}^{-1} \text{ rad}^{-2}$
Dihedral phase	$\pi \text{ rad}$
Dihedral amplitude	10 kJ mol^{-1}

Table 2. Prior width values for each parameter type.

The fourth term in the objective function is the regularization term that penalizes parameter deviations from their initial values. Since the force field parameters have different physical unit systems, the parameter deviations must be placed on the same footing by rescaling prior to computing the penalty function. The penalty function corresponds to a prior distribution in a Bayesian interpretation, and thus the rescaling factors for parameter deviations are equivalent to the prior widths. The results of the optimization do depend on the choice of prior widths, but in a much less sensitive way compared to the force field parameters themselves. Because the bond and angle terms are intended to model small harmonic displacements away from the lowest-energy structure, we chose small prior widths (approximately 10-20% of the parameters' intrinsic size) to enforce small parameter changes in the optimization. On the other hand, the dihedral terms are expected to vary more widely, as they represent a compromise between the

1
2
3 bonded and nonbonded parts of the force field. We thus chose the prior widths to be on the same
4 order as the parameter themselves. The full set of prior widths used in the optimization is given
5 in Table 2.
6
7
8
9

10 The objective function was minimized using a variation of the Levenberg trust-radius
11 method⁷⁵⁻⁷⁸ implemented in ForceBalance. A parameter update ($\mathbf{k}_{n+1} - \mathbf{k}_n$) is calculated as:

$$\mathbf{k}_{n+1} - \mathbf{k}_n = [\mathbf{H}|_{\mathbf{k}_n} + (\lambda - 1)^2 \mathbf{I}]^{-1} \mathbf{G}|_{\mathbf{k}_n} \quad (9)$$

12
13 where $G_i \equiv \frac{\partial}{\partial k_i} \chi^2$ and $H_{ij} \equiv \frac{\partial^2}{\partial k_i \partial k_j} \chi^2$ are the gradient and Hessian matrix of the objective
14
15
16
17
18
19
20
21
22
23
24 function in parameter space, and λ is a parameter that affects the length of the optimization step.
25
26 The Hessian is approximated using the Gauss-Newton method. For the calculations in this paper,
27
28 the objective function is much less expensive to evaluate than its derivatives – so a line search
29
30 over λ is performed rather than taking an optimization step of a fixed length. ForceBalance uses
31
32 the Brent method as implemented in SciPy⁷⁹ to perform the line search. The quadratic form of
33
34 the coefficient $(\lambda - 1)^2$ maps all λ values on the real line to nonnegative values and ensures that
35
36 the line search is well behaved.
37
38
39
40

41 COMPUTATIONAL METHODS

42
43 The *ab initio* reference calculations were carried out in a workflow involving several
44
45 software packages. The initial high-dimensional dihedral grid of structures was generated from
46
47 restrained simulated annealing simulations using the AMOEBA protein force field as
48
49 implemented in TINKER.⁸⁰ The recursive search over the two-dimensional dihedral grids was
50
51 performed using a Python program that interfaces with the Q-Chem 4.1 quantum chemistry
52
53 package⁸¹⁻⁸² and uses the Work Queue distributed computing library⁸³ to manage a large number
54
55
56
57
58
59
60

of Q-Chem calculations running in parallel. The calculations of final optimized structures, energies and gradients were performed in Psi4.⁸⁴ Frequencies were obtained in Psi4 via numerical differentiation of the analytic gradients.

The parameterization calculations were performed using ForceBalance via an interface to GROMACS 4.6.5,⁸⁵ and contained two fundamental types of MM calculations – single-point energy / gradient evaluations, and frequency calculations. In the frequency calculations, the MM energy was fully minimized using the L-BFGS algorithm prior to calculating the Hessian. ForceBalance also uses the Work Queue library to evaluate individual *targets* in parallel, providing a significant speed-up compared to running all of the MM calculations sequentially.

The validation calculations were performed using multiple software packages. The equilibrium sampling simulations initialized from the crystal structure were carried out using GROMACS 4.6.5 running on standard Linux HPC hardware. The analyses of the equilibrium simulations to calculate RMSD from the crystal structure and NMR scalar couplings / chemical shifts were carried out using the GROMACS analysis tools, the MDTraj trajectory analysis package,⁸⁶ and the ShiftX2 chemical shift prediction software⁸⁷.

The temperature replica exchange simulations were set up using the ParmEd software package⁸⁸ to convert the GROMACS topology files to AMBER format, carried out using the GPU-accelerated version of AMBER14⁸⁹ running on the OLCF Titan supercomputer, and analyzed using the cpptraj⁹⁰ and MDTraj⁹¹ software packages. The simulations of the denatured state ensemble were carried out on the Open Science Grid (OSG), a distributed computing network that utilizes donated idle CPU cycles from research computing facilities.⁹²

RESULTS AND DISCUSSION

Model	Bond	Angle	Dihedrals	Side Chains	N (Params)	MUE (kcal/mol)	Objective Function χ^2
-------	------	-------	-----------	-------------	--------------	----------------	-----------------------------

	Initial Parameters (A99SB)					2.78	38.0
Prelim 1	No	No	k_φ	No	69	1.69	16.8
Prelim 2	No	No	k_φ, φ_0	No	138	1.65	12.6
Prelim 3	k_b	k_θ	k_φ	No	210	1.34	11.9
A99SB-V	k_b, b_0	k_θ, θ_0	k_φ, φ_0	No	420	1.00	6.0
AMBER-FB15	k_b, b_0	k_θ, θ_0	k_φ, φ_0	k_φ, φ_0	1406	0.80	4.1

Table 3. Optimized objective function (χ^2) values in a preliminary run of ForceBalance using only the energies from the first two rows of Table 1. The results indicate that all parameter types have a significant impact on lowering the objective function.

Choice of optimization parameters. We assessed the significance of optimizing different types of parameters by testing the following choices: (1) including bond and angle parameters, (2) allowing side chain torsions to take on distinct parameter values, and (3) including equilibrium geometry parameters in addition to the force constants. We ran several optimizations using a simplified version of the objective function where only the (φ, ψ) dihedral scans were included (first row of Table 1). The results demonstrate that tuning the backbone dihedral parameters have a significant effect on decreasing the objective function (Table 3). Perhaps more surprising is the effect of bond and angle parameters; the first and third rows of Table 3 show that including the bond and angle force constants lower the objective function by ~30% compared to using only the dihedral force constants. Allowing the equilibrium geometry parameters to be optimized results in a further 50% decrease in the objective function as shown in the fifth row of Table 3. Based on these results, we decided to allow all parameter types to vary in our optimizations.

The model named A99SB-V is the optimized result using all of the A99SB bonded parameters and the data in Table 1. After adding some parameters corresponding to alternative protonation states of amino acids, the total number of adjustable parameters in A99SB-V was 434, and the mean unsigned error (MUE) of the potential across all of the dihedral scans was

1.90 kcal/mol. We also developed a variant of this force field where the side chain torsion parameters for different amino acids were all allowed to vary independently; this led to a decrease of 37% in the objective function, but the number of parameters increased greatly to 1406. Because this force field reproduced experimental results more accurately than A99SB-V and several other models in the validation calculations, we named it AMBER-FB15 and recommend it here for broader use.

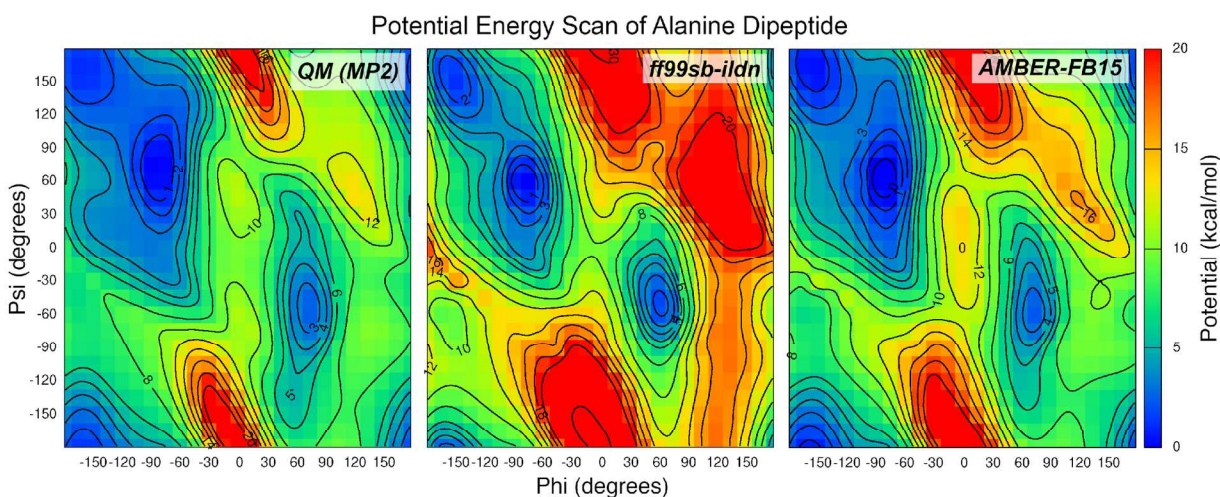
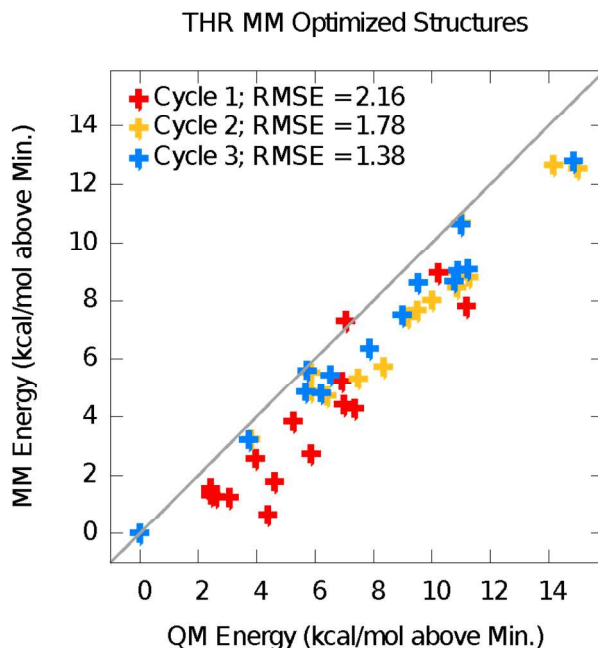


Figure 1. Plot of the potential energy in alanine dipeptide calculated for energy-minimized structures at the MP2/aug-cc-pVTZ level with the (ϕ, ψ) dihedral angles constrained. Color indicates the relative potential energy with respect to the minimum.

Optimized parameter values. Figures S1-S3 in the Supporting Information show the original and optimized parameter values in AMBER-FB15 grouped by parameter type. The optimized equilibrium bond and angle parameters are all within 5% of their initial values and fall very close to the straight line. Bond and angle force constants show slightly larger deviations; some force constants involving the amide bond are reduced by up to 10% from their initial values. The torsion phases and amplitudes are more widely distributed, largely because the initial guesses for side-chain parameters are set to zero. With few exceptions, the equilibrium torsion phases fall within $\frac{\pi}{6}$ radians (30 degrees) of their initial values, and the torsion amplitudes seldom change

1
2
3 by more than 4 kJ/mol (1.0 kcal/mol). The largest parameter deviations are observed for arginine
4
5 and lysine, which possess charged side chains; this is expected due to the especially strong
6
7 electrostatic interactions in the gas-phase QM calculations, which contributes large terms to the
8
9 objective function. We note in passing that the usage of gas-phase QM data is most likely to fail
10
11 for charged systems, but choosing the most appropriate QM method to fit a condensed-phase
12
13 fixed charge model remains an important challenge.⁶¹
14
15

16
17 **Quality of fit.** Figure 1 shows the potential surface of alanine dipeptide evaluated at the
18
19 constrained energy minima. As expected, AMBER-FB15 produces a closer fit to the QM energy
20
21 surface relative to A99SB-ILDN (equivalent to A99SB for alanine). Comparison of the QM and
22
23 MM surfaces reveals that A99SB-ILDN fits the low-energy regions (in blue) much more
24
25 accurately than the high-energy regions (in red), and high-energy regions are systematically
26
27 overpredicted. By contrast, AMBER-FB15 significantly reduces (but does not eliminate) the
28
29 overprediction of the energy, and the low-energy basins with energy less than 5 kcal/mol above
30
31 the minimum are significantly broadened. We expect that the broader energy basins in low-
32
33 energy regions will lead to larger thermodynamic fluctuations at finite temperatures, which may
34
35 result in more accurate predictions (as explored in the validation simulations).
36
37
38
39
40
41
42
43
44
45
46
47
48
49
50
51
52
53
54
55
56
57
58
59
60



25 **Figure 2.** MM vs. QM potential energies for MM-optimized geometries of threonine dipeptide.
26 Each data point corresponds to a local energy minimum predicted by the force field. The Cycle 1
27 parameters were fitted to QM data from the torsion scans only. The QM data points at the local
28 minima of Cycle 1 are added to the optimization of the Cycle 2 parameters. Cycle 3 is the final
29 parameter set. The spurious MM energy minima (points far below the diagonal line) are
30 eliminated in later cycles.
31

32
33 Figure 2 shows the comparison of QM and MM energies at the local minima of the optimized
34 force field for threonine dipeptide. The initial parameter set (red crosses) predicts the relative
35 energies with a RMS error of 2.16 kcal/mol, and several local minima are within 2 kcal/mol of
36 the lowest-energy structure; by contrast the QM relative energies are significantly higher,
37 ranging between 2 and 6 kcal/mol above the minimum. These local minima with spuriously low
38 relative energies are biased towards higher probability in finite-temperature simulations, which
39 could adversely perturb the equilibrium structure. These local minima are added to the objective
40 function (third term in Equation (4)) to obtain a new set of parameters, which predicts a new set
41 of local minima with relative energies that match the QM calculations much more closely
42 (yellow crosses). Repeating the addition of local minima to the objective function leads to
43
44
45
46
47
48
49
50
51
52
53
54
55
56
57
58
59
60

1
2
3 smaller improvements in the predicted relative energies (blue crosses), and the resulting
4 parameter set is kept as the final version.
5
6

7 *Equilibrium properties.*

8
9
10 After a force field is developed, the predictive power of the model is validated using a set of
11 test properties not used during the fitting procedure. In order to assess the ability of AMBER-
12 FB15 to reproduce equilibrium properties of folded proteins, we ran simulations of 8 proteins:
13
14
15 the third IgG-binding domain from streptococcal protein G, abbreviated as *GB3* (PDB ID: 1IGD),
16
17
18 *acetyltransferase* from the COG2388 family (2EVN), *lambda repressor* taken from the
19
20
21 repressor-operator complex (1LMB), *lysozyme* from bacteriophage lambda (1AM7), N-terminal
22
23
24 Domain of Ribosomal Protein L9 or *NTL9* (2HBA), a variant of the *Trp-cage* miniprotein (2JOF),
25
26
27 *ubiquitin* (1UBQ), and chicken villin subdomain HP-35 or *villin headpiece* (2F4K). Each protein
28
29
30 was simulated at 298.15 K using 7 force fields and 4 water models. All proteins were solvated in
31
32
33 a cubic water box with a side length of 62 Å. Na⁺ and Cl⁻ ions were added to neutralize the
34
35
36 proteins using the parameters of Åqvist;⁹³ the ubiquitin simulations had 12 additional ion pairs
37
38
39 corresponding to an ionic strength of ~50 mM. For each simulation, the RMSD of the protein
40
41
42 backbone to the PDB reference was computed using the residue intervals specified in Table S1,
43
44
45 and the RMSD probability density function estimated via a kernel density estimate (KDE). In
46
47
48 order to separate thermodynamic fluctuations from shifts in the equilibrium structure, we
49
50
51 calculated the Cartesian-averaged protein backbone coordinates (after alignment to remove
52
53
54 translation and rotation) and calculated the RMSD to the crystal structure; these values are
55
56
57 typically lower than mean RMSD values. This data is illustrated for three proteins in Figure 3,
58
59
60 and the rest are provided in Figure S4. Two protonation states of lysozyme were considered –
one state is determined using the pKa values of the amino acids, and the other is determined

1
2
3 using the H⁺⁺ pKa prediction software;⁹⁴ the simulation results were not significantly different
4
5 and only the H⁺⁺ simulation results are shown here. Each of the 252 simulations was performed
6
7
8 for at least 300 ns with an average trajectory length of 500 ns.
9

10 Simulating a protein in water at ambient conditions may not reproduce the crystallographic
11 structure exactly, due to differences in the environment and thermodynamic ensemble. However,
12
13 crystal structures are often the best structural data available, and it is reasonable to assume that
14
15 proteins in water stay reasonably close to the crystal structure unless experiments show strong
16
17 evidence to the contrary. Thus, the RMSD of the simulation trajectory to the crystal structure is
18
19 routinely considered as an important qualitative validation test of a protein force field, and
20
21 simulations that deviate significantly from the crystal structure in a short time (i.e. on the sub-
22
23 microsecond timescale) are interpreted as evidence of force field errors.
24
25
26
27
28
29
30
31
32
33
34
35
36
37
38
39
40
41
42
43
44
45
46
47
48
49
50
51
52
53
54
55
56
57
58
59
60

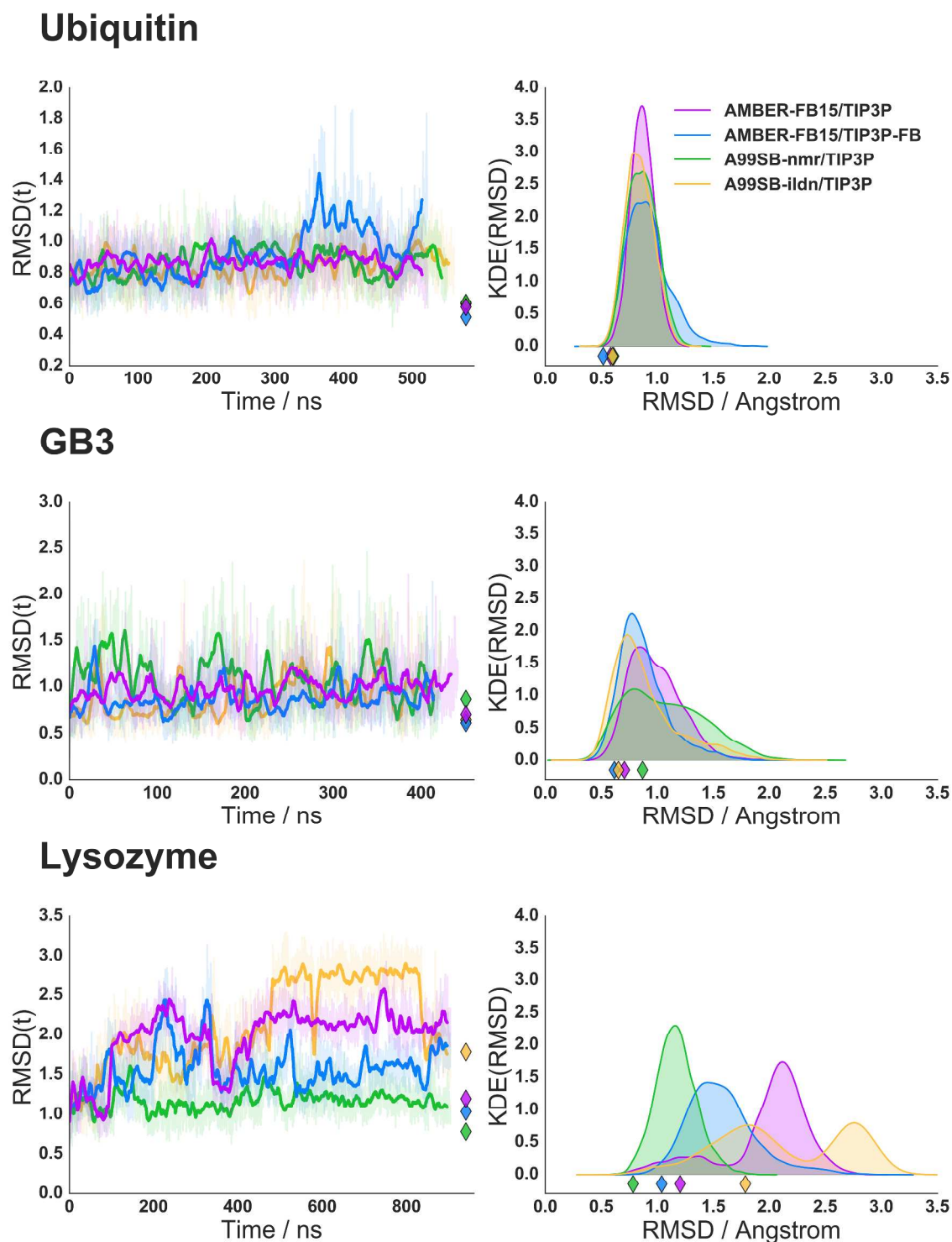


Figure 3. Time series of RMSD to the experimental crystal structure for three proteins and four simulations. The right panels show Gaussian kernel density estimates of the RMSD values. The diamond markers indicate the RMSD to the crystal structure using the Cartesian-averaged protein backbone conformations over the whole simulation.

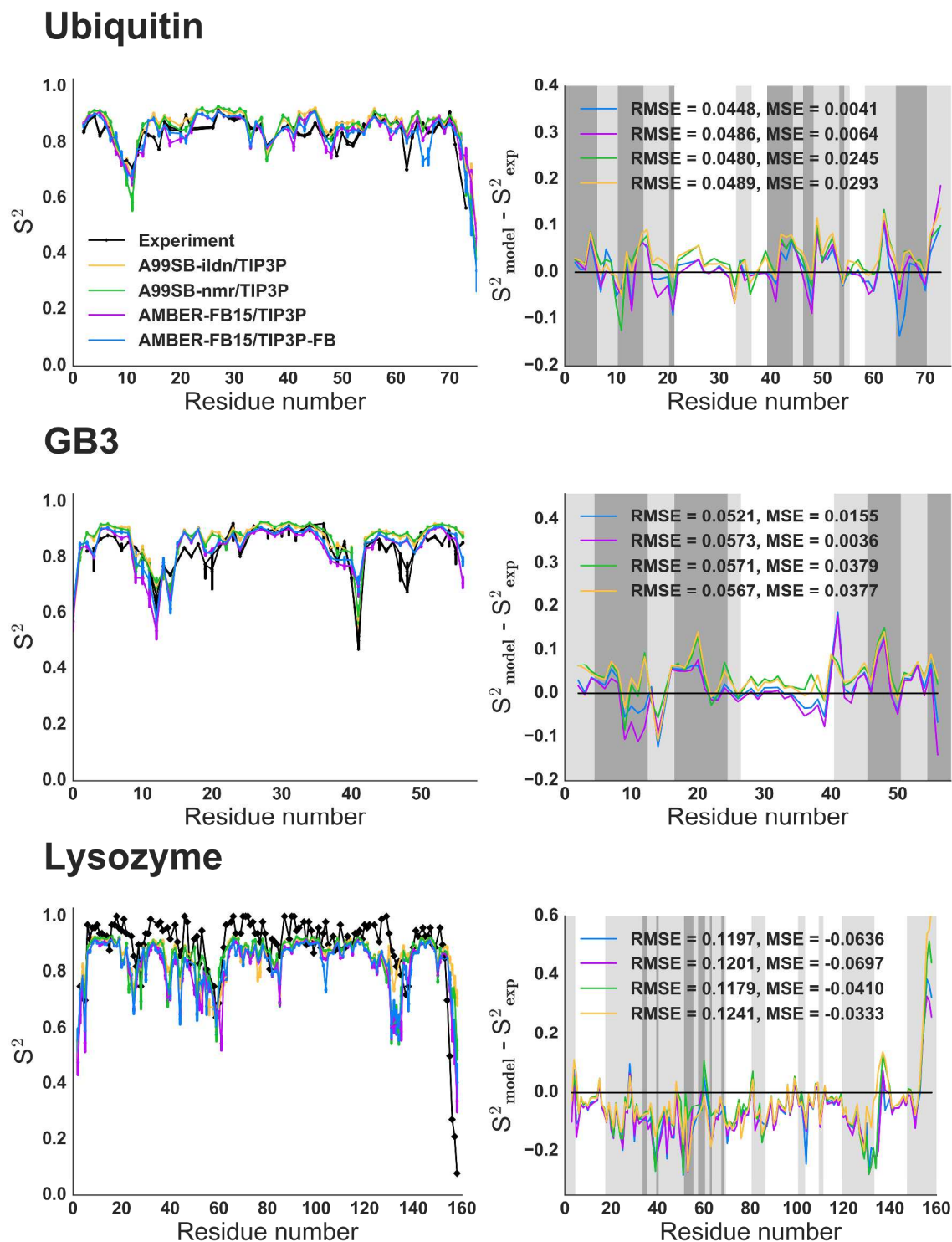


Figure 4. Lipari-Szabo S^2 order parameters and error residuals compared to experimental NMR measurements. The root-mean-squared error (RMSE) and mean signed error (MSE) of the simulated observables with respect to experiment are given in the legends. The background of the error residual plots are colored according to secondary structure as determined by DSSP analysis (white, helix; light gray, coil; dark gray, strand).

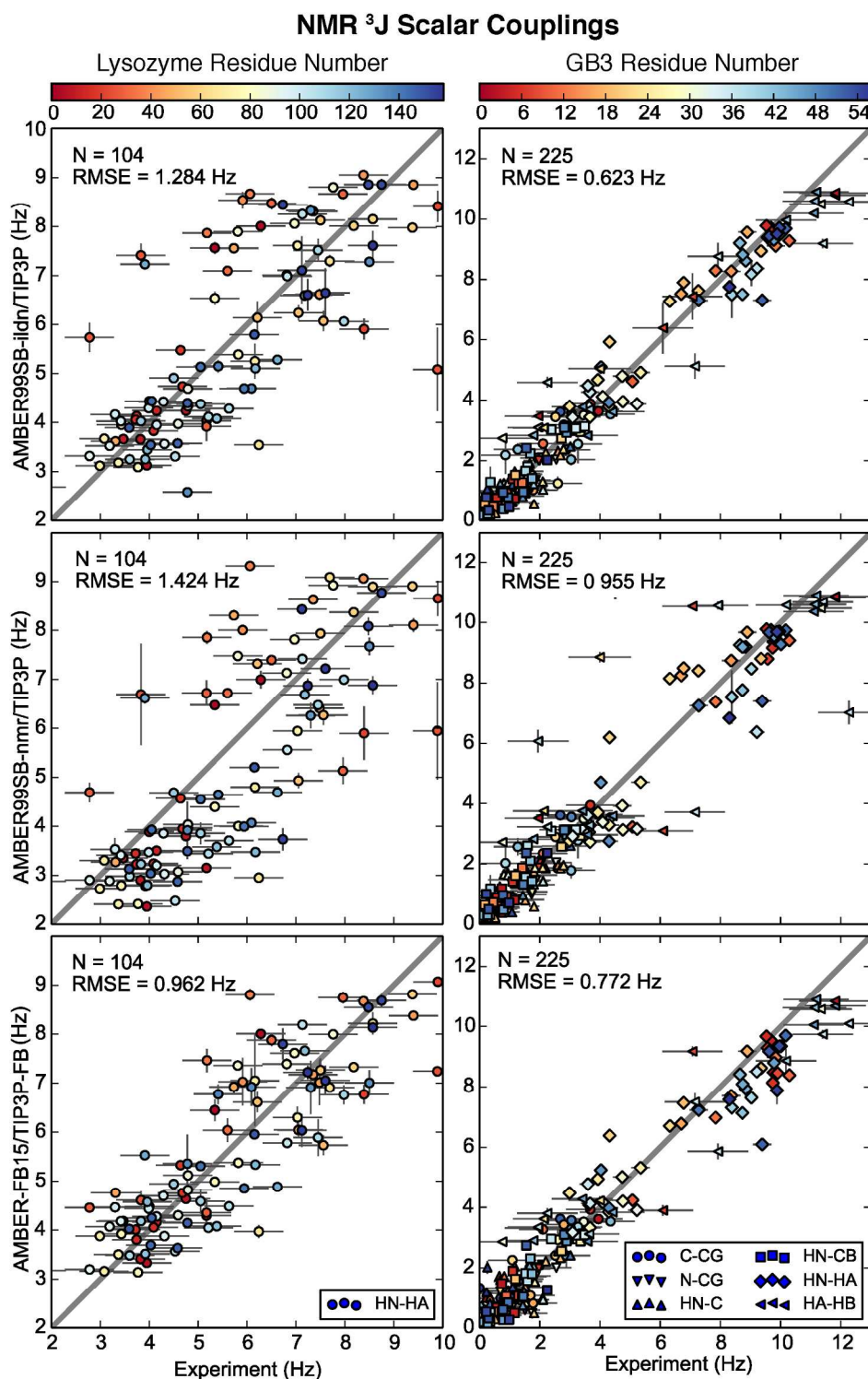


Figure 5. Scatter plots of experimental vs. calculated NMR three-bond scalar couplings. Two proteins are shown (left: bacteriophage lysozyme, PDB ID 1AM7, right: GB3, PDB ID 1IGD) and three models (top, AMBER99SB-ildn/TIP3P; middle, AMBER99SB-nmr/TIP3P; bottom, AMBER-FB15/TIP3P-FB from this work.) Symbols represent the atom pair involved in the coupling, and colors represent the position of the residue in the protein sequence.

1
2
3
4
5
6
7
8
9
10
11
12
13
14
15
16
17
18
19
20
21
22
23
24
25
26
27
28
29
30
31
32
33
Figure 3 shows the RMSD time series for three proteins simulated using four combinations of the protein force field and water model. The protein remains folded in all simulations, and the simulations differ in terms of the overall RMSD to the crystal structure. In the case of ubiquitin, all models have nearly identical RMSD distributions, except for AMBER-FB15/TIP3P-FB which has a small shoulder in the distribution indicating more flexibility in the backbone (also see Supporting Figure S4). In lysozyme and GB3, AMBER-FB15 predicts an RMSD value in between that of A99SB-ILDN and A99SB-NMR; when the water model is changed to TIP3P-FB, the RMSD distribution is shifted to lower values. In all of the simulations except for acetyltransferase, the averaged backbone Cartesian coordinates of the AMBER-FB15/TIP3P-FB remains very close to the crystal structure with a RMSD of 1.0 Å or less. The RMSD distribution for lysozyme is significantly broader than ubiquitin and GB3, and the A99SB-ILDN simulation possesses some bimodal character; this may indicate larger conformational changes on timescales exceeding microseconds that have not been fully sampled in our calculations.

34
35
36
37
38
39
40
41
42
43
44
45
46
47
48
49
50
51
52
53
54
55
56
57
58
59
60
To enrich our understanding of model dependence on equilibrium stability, Lipari-Szabo S^2 order parameters were computed for proteins and compared to the available experimental data. Previous studies have shown that simulation lengths exceeding 100 ns are required for accurate estimation of these order parameters,⁹⁵ a condition that is satisfied by our calculations. These simulated observables were determined from the trajectories using the isotropic reorientational eigenmode dynamics⁹⁶ (iRED) as implemented in the cpptraj program⁹⁰ for windows of length 2, 4, and 8 ns. The per-residue deviation from the experimental NMR measurements are shown in Figure 4. These order parameters measure the orientational disorder of the protein backbone N-H vectors on the sub-nanosecond timescale. For all three proteins simulated, we found AMBER-FB15 to produce lower S^2 values by 0.02–0.03 compared to A99SB-ILDN and A99SB-NMR. In

1
2
3 the cases of ubiquitin and GB3, AMBER-FB15 predicts significantly lower mean signed errors
4 (MSE), indicating that the increased disorder is consistent with experiment. AMBER-
5
6 (MSE), indicating that the increased disorder is consistent with experiment. AMBER-
7
8 FB15/TIP3P-FB predicts the smallest root mean squared errors (RMSE) for these two proteins.
9
10 In the case of lysozyme, the experimental measurements have many S^2 values in excess of 0.9,
11
12 higher than all of the simulated values; here AMBER-FB15 predicts the largest MSE although
13
14 the RMSE is still very close to those of A99SB-ILDN and A99SB-NMR. An earlier study by
15
16 Smith and coworkers applied an upper threshold of 0.9 to the experimental order parameters;⁹⁷⁻⁹⁸
17
18 when using this threshold, all of the RMSE values are significantly reduced with AMBER-FB15
19
20 producing the lowest error (Figure S5).
21
22
23

24
25 The protein structure from equilibrium MD can also be related to NMR experiments using
26
27 empirical relations to map the three-dimensional structure to the NMR observable. Three-bond J-
28
29 couplings are often used to compare simulated dihedral angles to experiment; this requires the
30
31 use of an empirical Karplus relation, which is developed by fitting the crystal structure backbone
32
33 and side chain dihedral angles to the NMR observable. The comparison of calculated to
34
35 experimental NMR observables is an important validation test, but perfect agreement is not
36
37 expected due to the assumptions and residual errors of the empirical model. Furthermore,
38
39 because the Karplus relations implicitly include some effects of dynamics in mapping the crystal
40
41 structure to the solution NMR experiment, using molecular dynamics snapshots as an input to
42
43 this mapping results in double-counting the effects of dynamics⁹⁹⁻¹⁰⁰ which may lead to
44
45 additional errors.
46
47
48
49

50
51 Figure 5 shows the RMS error of the computed NMR three-bond J-couplings compared to
52
53 experiments for two proteins, bacteriophage lysozyme and GB3. The recommended model in this
54
55 work (AMBER-FB15/TIP3P-FB) is compared to A99SB-ildn and A99SB-nmr, both with the
56
57
58
59
60

1
2
3 TIP3P water model. From examining the left column, the AMBER-FB15/TIP3P-FB model
4
5 predicts the backbone J-couplings of bacteriophage lysozyme in closer agreement with
6
7 experiment. The right column shows that A99SB-ildn and AMBER-FB15 both have improved
8
9 results over A99SB-nmr, which could be explained by the explicit parameterization of side chain
10
11 torsional potentials. We also calculated J-couplings for two other proteins (ubiquitin and NTL9,
12
13 Figure S6), and found small differences between the RMSE values compared to experiment on
14
15 the order of 0.1 – 0.2 Hz. Although the J-couplings shown here were calculated using the
16
17 Karplus parameters of Ruterjans and coworkers,¹⁰¹⁻¹⁰² we note that the RMSE values change on
18
19 the order of 0.1 when using the parameters of Bax and coworkers¹⁰³⁻¹⁰⁴ and does not affect the
20
21 qualitative interpretation of the results.
22
23
24
25

26
27 The NMR chemical shifts on ¹H, ¹³C and ¹⁵N can be predicted from MD trajectories using
28
29 empirical models such as SHIFTX2,⁸⁷ which take into account a rather large number of
30
31 geometric features and fitting parameters to represent the local chemical environment. Similar to
32
33 Karplus relations for J-couplings, the chemical shift models are fitted using structural input from
34
35 crystallography. The RMSE of the predicted chemical shifts are plotted in Figures S7 and S8.
36
37 We observed that the prediction quality depends heavily on the protein, in contrast to the case of
38
39 three-bond J-couplings. The RMSE is often within the range of the intrinsic error of SHIFTX2
40
41 itself; in an extreme case, the RMSE for ubiquitin is smaller than the SHIFTX2 intrinsic error,
42
43 which corresponds to χ^2 statistics of less than one and does not reflect the differences between
44
45 force fields in a meaningful way. From this, we concluded that the chemical shift predictions
46
47 were insufficient to distinguish AMBER-FB15 from the literature models.
48
49
50
51
52

53 The results in this section show that AMBER-FB15 / TIP3P-FB does not degrade the
54
55 accuracy of simulating proteins in their native structure at ambient conditions, which is an
56
57
58
59
60

1
2
3 important validation test for any modern protein force field. Our claim is limited to the systems
4 and time scales studied in this paper, but it lends important credibility to this model for future
5 simulations of interesting biomolecular problems. Furthermore, equilibrium properties are no
6 longer a frontier for protein force field development, with temperature dependence and
7 characterization of the denatured state ensemble being much more important. We will focus our
8 discussion on these important frontiers in the next section.
9

10
11
12
13
14
15
16
17 **Temperature dependence.** Several of the most popular protein force fields in the past ten years
18 have succeeded at reproducing equilibrium structures of folded proteins but failed to predict an
19 accurate temperature dependence of the structural ensemble. In previous work, Best and
20 Hummer proposed the A03* and A99SB* models which were directly fitted to reproduce helical
21 fractions at finite temperature;¹⁰⁵ more recently, Wu and coworkers showed improved
22 performance for temperature dependence adding extra 1-5 and 1-6 Lennard-Jones interaction
23 terms and fitting the potentials to experimentally derived free energy distributions.⁷³ Here we
24 consider the predicted temperature dependence of AMBER-FB15 for two model systems; Ac-
25 (AAQAA)₃-NH₂ (abbreviated here as AAQAA₃), a 15-residue peptide with partial α -helical
26 character at room temperature, and CLN025, a 10-residue peptide with mostly β -hairpin structure.
27 These two proteins have a significant temperature dependence of the folded fraction in the range
28 280 – 370 C as measured by circular dichroism¹⁰⁶ and temperature-dependent infrared
29 spectroscopy experiments.¹⁰⁷ The results presented in this section are taken from NVT replica
30 exchange simulations as implemented in AMBER.¹⁰⁸⁻¹⁰⁹ The published simulation results of
31 several protein force fields from the last few years are also presented including FF12MC,¹¹⁰
32 OPLS3¹¹¹, CHARMM22*,¹¹² and the AMBER force fields ff12sb and ff14sb.⁷⁴
33
34
35
36
37
38
39
40
41
42
43
44
45
46
47
48
49
50
51
52
53
54
55
56
57
58
59
60

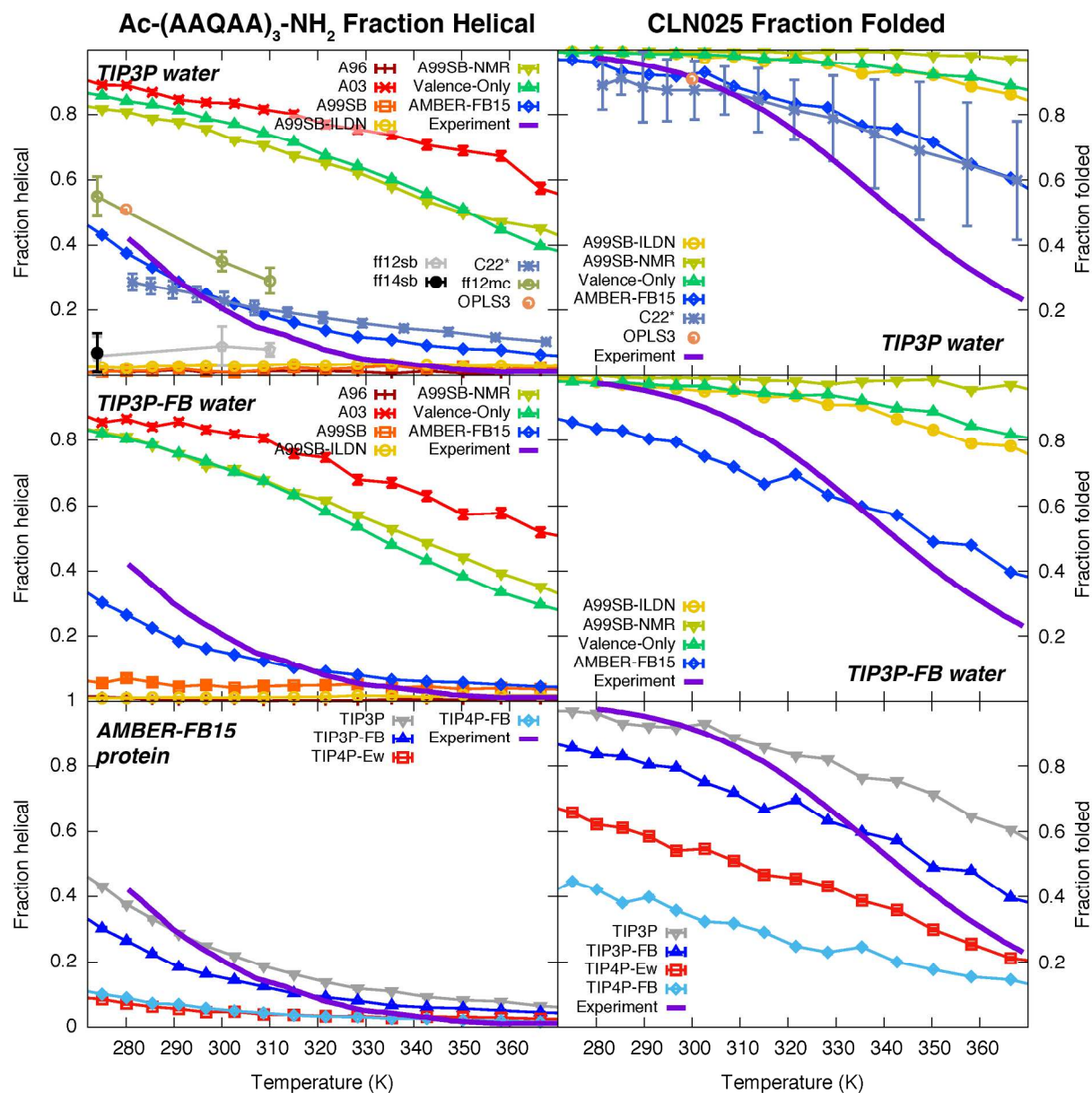


Figure 6. Temperature dependence of secondary structure for two small peptides as a function of temperature and several force field / water model combinations. The performance of the AMBER-FB15 / TIP3P-FB model combination is the dark blue trace in the middle row. Left column: The helical fraction of Ac-(AAQAA)₃-NH₂. Right column: The fraction folded of CLN025. Top row: Comparison of multiple protein force fields using TIP3P water model. Middle row: Same comparison using TIP3P-FB water model. Bottom row: Comparison of four water models using AMBER-FB15 protein force field.

The left column of Figure 6 shows the temperature dependence of Ac-(AAQAA)₃-NH₂ for combinations of protein force fields and water models compared to experiment. Our results for

1
2
3 published models show a high degree of consistency compared with existing protein force field
4 validation studies of temperature dependence performed by Lindorff-Larsen and coworkers.¹¹³
5
6 The top left and middle left panels compare seven protein force fields using the TIP3P and
7 TIP3P-FB models respectively. The data indicates that protein force fields developed to
8 reproduce equilibrium properties of folded proteins may fail to describe the temperature
9 dependence of partially folded proteins; the A99SB and A99SB-ildn force fields significantly
10 underestimate the α -helical fraction whereas A99SB-nmr significantly overestimates it. The two
11 parameter sets discussed in this paper, A99SB-V and AMBER-FB15, also differ significantly in
12 their temperature dependence. A99SB-V overestimates the helical fraction and behaves similarly
13 to A99SB-nmr whereas AMBER-FB15 has a temperature dependence mostly consistent with the
14 experiment.
15
16
17
18
19
20
21
22
23
24
25
26
27
28

29 The right column of Figure 6 shows temperature dependence plots for the CLN025 peptide, a
30 small model of a β -hairpin. Due to the high cost of these simulations, we skipped the older
31 models (A96, A03 and A99SB) and compared four protein force fields only. The top right and
32 middle right panels show that A99SB-ildn and A99SB-nmr both overestimate the folded fraction,
33 in contrast to the results for Ac-(AAQAA)₃-NH₂ where A99SB-ildn and A99SB-nmr are on
34 either side of the correct result. AMBER-FB15 again comes closest to reproducing the
35 experimental result.
36
37
38
39
40
41
42
43
44
45

46 The bottom left panel of Figure 6 compares temperature trends of Ac-(AAQAA)₃-NH₂ using
47 the AMBER-FB15 protein force field and four different water models. The choice of water
48 model affects the helical content; the simulations using TIP3P predict the most helical content,
49 followed by TIP3P-FB; the best agreement with experiment is given by TIP3P below 300K and
50 TIP3P-FB above 300K. By contrast, the simulations using TIP4P-Ew and TIP4P-FB predict a
51
52
53
54
55
56
57
58
59
60

1
2
3 much lower helical content. In a similar fashion, the bottom right panel of Figure 6 shows the
4 temperature trends in the folded fraction of CLN025 using the AMBER-FB15 force field and
5 four water models. The TIP3P simulations predict the highest folded fraction, followed by
6 TIP3P-FB, then TIP4P-Ew and TIP4P-FB. Figure S9 shows that using the TIP4P-Ew and TIP4P-
7 FB water models have the effect of decreasing the amount of protein structure for all seven
8 protein force fields. The best overall agreement with experiment is given by the AMBER-
9 FB15/TIP3P-FB simulations.

10
11
12
13
14
15
16
17
18
19
20 The effect of changing the water model on peptide stability is an interesting feature of the
21 simulations. Clearly, the accuracy of the protein temperature dependence does not depend
22 strongly on the accuracy of the water model, as both the TIP4P-Ew and TIP4P-FB models are
23 highly accurate for computing the properties of water. The ability of protein simulations to
24 accurately reproduce temperature dependence with TIP4P-Ew has been shown for model
25 peptides where abundant NMR data is available, requiring changes in only one backbone
26 dihedral parameter.¹¹⁴ Moreover, the nonbonded protein parameters of the protein were not
27 optimized, which will certainly have a strong effect on the temperature dependence. We expect
28 that improved derivations of point charge models from quantum chemistry calculations^{41,61} and
29 accompanying reparameterization of the Lennard-Jones interaction terms¹¹⁵ will produce more
30 accurate descriptions of temperature dependence for realistic water models; these efforts will
31 likely require re-optimization of the torsion parameters, as the 1-4 electrostatics and Lennard-
32 Jones terms contribute the major part of the torsional potential in the AMBER force field
33 definition.¹¹⁶ In light of all these considerations, it is still instructive to search for other trends in
34 the water models that correlate well with the temperature dependence trends observed here.
35
36
37
38
39
40
41
42
43
44
45
46
47
48
49
50
51
52
53
54
55
56
57
58
59
60

When CLN025 is simulated with AMBER-FB15 (and when AAQAA₃ is simulated with A99SB-V), the helical/folded fraction takes on a wide range of values between 0.1 and 0.9; there is also a clear trend of peptide stability that goes as TIP3P > TIP3P-FB > TIP4P-Ew > TIP4P-FB. We could not find a significant correlation between the peptide stability and the basic properties of the water models, such as the internal energy or magnitude of the dipole moment. On the other hand, the peptide stability was significantly correlated with the average interaction energy between protein and water (Figure 7).

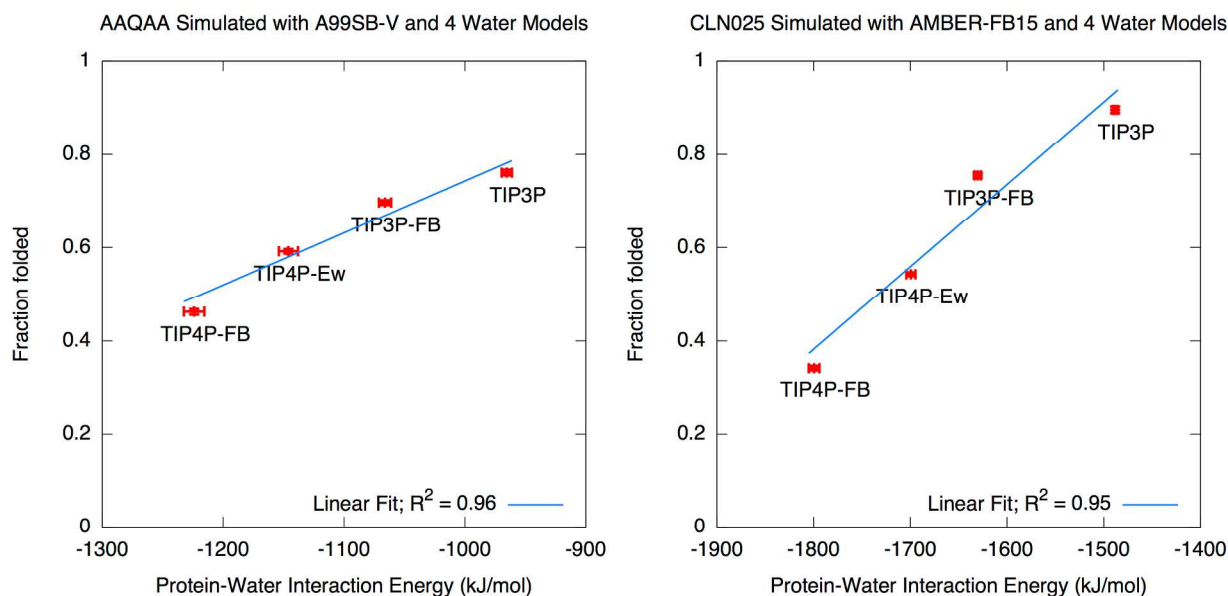


Figure 7. Correlation between average protein-water interaction energy and fraction of secondary structure. Left: AAQAA simulated with A99SB-V (left). Right: CLN025 simulated with AMBER-FB15 (right). Each plot contains four simulations with four water models. Error bars represent one standard error.

We tested the effects of changing the water model “in-place” by replacing the water model in the simulation trajectory, creating a 4x4 grid where the simulation trajectory using model X was used to calculate the protein-water interaction using model Y. We found that (1) changing the water model from TIP3P→TIP3P-FB→TIP4P-EW→TIP4P-FB increased the protein-water interaction strength independent of which trajectory was used, and (2) the conformational

ensembles from TIP3P→TIP3P-FB→TIP4P-EW→TIP4P-FB had increasingly strong protein-water interactions independent of which water model was used (Figure S10). Our analysis indicates that having stronger water-protein interactions *causes* proteins to become less stable, consistent with previous studies on protein-water interactions.¹¹⁴

While this is an encouraging sign of progress, we also note that all of the potentials underestimate the slope of the temperature dependence. One possible reason is that the simulated and experimental ensembles are different; the experiment is performed at constant pressure whereas the replica exchange simulations could only be done in the NVT ensemble. If the simulations had been run in the NPT ensemble instead, the density of water would have decreased at higher temperatures, which may have an effect on the helical fraction. Another possibility is the pairwise additive approximation from the force field, which neglects many-body effects such as those arising from explicit electronic polarization. Including the electronic polarizability may increase the cooperativity of helix formation and lead to a steeper temperature dependence.¹¹⁷ We intend to apply this parameterization strategy and *ab initio* data set toward the parameterization of a polarizable force field in forthcoming work.

	TIP3P	TIP3P-FB	TIP4P-EW	TIP4P-FB
A96	1.80 (0.10)	1.99 (0.16)	1.92 (0.10)	1.88 (0.08)
A03	1.42 (0.06)	1.77 (0.15)	1.65 (0.08)	1.79 (0.12)
A99SB	1.69 (0.11)	1.83 (0.14)	1.75 (0.09)	1.84 (0.11)
A99SB-ILDN	1.70 (0.13)	1.77 (0.12)	1.82 (0.11)	2.01 (0.11)
A99SB-NMR	1.68 (0.10)	1.82 (0.10)	1.75 (0.11)	1.79 (0.08)
A99SB-V	1.64 (0.08)	1.91 (0.13)	1.80 (0.10)	1.75 (0.08)
AMBER-FB15	1.47 (0.07)	1.77 (0.10)	1.75 (0.08)	1.88 (0.10)

Table 4. Average radius of gyration (R_g) of the denatured state ensemble of GB3 simulated using seven protein models and four water models, started from an ensemble of initial conditions with an average R_g value of 1.65 nm. Bold entries denote average R_g values in excess of 1.9 nm. The experimental measurements are 2.2 nm (FRET) and 2.6 nm (SAXS) from Ref. 121.

1
2
3 *Denatured state ensemble.* A current frontier in protein simulations is the description of the
4 denatured state ensemble (DSE), a vast conformational space where protein conformations are
5 extended relative to the native state.¹¹⁸ The DSE is closely connected with intrinsically
6 disordered proteins,¹¹⁹ which do not possess a well-defined native state and may play important
7 roles in neurological disorders.¹²⁰ Experimentally, the average radius of gyration (R_g) of
8 denatured proteins may be inferred from Forster resonance energy transfer (FRET) and small
9 angle X-ray scattering (SAXS) data.¹²¹ Simulations of the DSE have been shown to produce
10 structures that are collapsed relative to experiment;¹²¹ efforts to uniformly increase the strength
11 of protein/water interactions have shown some promising results,¹²³ though more studies are
12 needed to assess whether this approach applies equally well to the diverse sequences of IDPs.¹²⁴
13
14
15
16
17
18
19
20
21
22
23
24
25
26

27 Here we simulated the DSE of GB3 by first denaturing the protein by running 20 ns
28 simulations at 600 K for all 28 protein / water model combinations; we then extracted five
29 snapshots at 1 ns intervals from the end of each trajectory, creating 140 initial structures in total
30 with an average R_g value of 1.65 nm. We then launched 10 ns simulations for each of the 140
31 initial conditions for all 28 protein / water model combinations, a total of 3,960 simulations total.
32 2,226 of these 3,960 simulations ran to completion, representing about 800 ns of simulation time
33 for each protein / water model combination; although 1,734 of the simulations did not run to
34 completion, those that finished were spread as evenly as possible over the 28 protein / water
35 model combinations. Our results are summarized in Table 4, which shows that all tested protein
36 models systematically underestimate the radius of gyration in comparison with experiment.
37 Although the short simulation time of 10 ns is far from sufficient from sampling this large
38 ensemble,¹²² the calculated R_g values demonstrate some significant differences from the initial
39 values and between the water models; for example, the TIP3P simulations predict significantly
40
41
42
43
44
45
46
47
48
49
50
51
52
53
54
55
56
57
58
59
60

1
2
3 more compact distributions on average 0.2 nm smaller than TIP3P-FB. The TIP3P-FB, TIP4P-
4
5
6
7
8
9
10
11
12
13
14
15
16
17
18
19
20
21
22
23
24
25
26
27
28
29
30
31
32
33
34
35
36
37
38
39
40
41
42
43
44
45
46
47
48
49
50
51
52
53
54
55
56
57
58
59
60

more compact distributions on average 0.2 nm smaller than TIP3P-FB. The TIP3P-FB, TIP4P-Ew and TIP4P-FB simulations produce average R_g values that are larger than the initial conditions (where $\langle R_g \rangle = 1.65$ nm), but they are all significantly less than the experimental values derived from FRET or SAXS measurements (2.2 and 2.6 nm respectively). The data indicates that the R_g values from TIP3P-FB, TIP4P-Ew, and TIP4P-FB simulations are moving in the correct direction, but longer simulations are needed to discern whether any of them are in quantitative agreement with the experimental DSE.

Conclusion

The AMBER-FB15 protein force field combines the well-established model of intermolecular interactions from AMBER94 with a systematic and thorough optimization of the intramolecular terms. The key difference in the optimized result is a significant lowering of the potential in regions away from the energy minima, which is expected to yield greater flexibility in finite temperature simulations. Our validation studies found that the predictions of equilibrium thermodynamic properties were equivalent in accuracy to published models, and the predictions of temperature dependence were significantly improved. Replacing the TIP3P water model with the updated TIP3P-FB model resulted in overall improved accuracy of the temperature dependence predictions. Our simulations of the denatured state ensemble were insufficient to conclude whether any of the models are in quantitative agreement with experiment, although the newer water models predicted larger R_g values in closer agreement with experiment compared to when TIP3P is used. Supported by the evidence in this paper, we are optimistic that the model combination AMBER-FB15/TIP3P-FB will yield accurate predictions in simulations of proteins, particularly when fluctuations away from equilibrium, conformational changes and/or temperature dependence are expected to play important roles.

Acknowledgements

We acknowledge Dave Case, Dave Cerutti, John Chodera and members of the Chodera Lab for insightful discussions. We acknowledge Christina Redfield for sharing the order parameter data for bacteriophage lysozyme. The simulations of protein temperature dependence were performed on the Titan supercomputer at the Oak Ridge Leadership Computing Facility (OLCF). We acknowledge Jason Swails for providing assistance with the ParmEd software package which enabled the temperature dependence simulations on Titan. The simulations of the denatured state ensemble used computational resources provided by the Open Science Grid (OSG). We acknowledge Miron Livny and the OSG Team for providing this resource and for their support. The Pande Group is broadly supported by grants from the NIH (R01 GM062868 and U19 AI109662) as well as gift funds and contributions from Folding@home donors. KAB acknowledges support from NIH grant P30CA008747, the Sloan Kettering Institute, and Starr Foundation grant I8-A8-058. THG acknowledges support from the NSF under grant CHE-1363320. TJM acknowledges support from NSF (ACI-1450179).

Disclosure

KAB is currently an employee of Counsyl, Inc.

VSP is a consultant and SAB member of Schrodinger, LLC and Globavir, sits on the Board of Directors of Omada Health, and is a General Partner at Andreessen Horowitz.

TJM is a co-founder of PetaChem, LLC.

Supporting Information Available. Scatter plots of original and optimized force field parameters for AMBER-FB15; RMSD time series for simulated proteins not shown in the main text; NMR S^2 order parameter calculation for lysozyme with thresholded experimental value; NMR 3J couplings for ubiquitin and NTL9; summaries of RMS errors in predicted chemical

shifts; temperature dependence plots for AAQAA and CLN025 with 4-point water models; additional tables and figures describing protein-water interaction energies.

Bibliography

1. Bash, P. A.; Field, M. J.; Davenport, R. C.; Petsko, G. A.; Ringe, D.; Karplus, M., Computer Simulation and Analysis of the Reaction Pathway of Triosephosphate Isomerase. *Biochemistry-U.S.* **1991**, *30* (24), 5826-5832.
2. Gao, J., Catalysis by Enzyme Conformational Change as Illustrated by Orotidine 5' - Monophosphate Decarboxylase. *Current Opinion in Structural Biology* **2003**, *13* (2), 184-192.
3. Ridder, L.; Mulholland, A. J.; Rietjens, I. M. C. M.; Vervoort, J., A Quantum Mechanical/Molecular Mechanical Study of the Hydroxylation of Phenol and Halogenated Derivatives by Phenol Hydroxylase. *J. Am. Chem. Soc.* **2000**, *122* (36), 8728-8738.
4. Wu, N.; Mo, Y.; Gao, J.; Pai, E. F., Electrostatic Stress in Catalysis: Structure and Mechanism of the Rnzyme Orotidine Monophosphate Decarboxylase. *Proceedings of the National Academy of Sciences* **2000**, *97* (5), 2017-2022.
5. Jindal, G.; Warshel, A., Exploring the Dependence of QM/MM Calculations of Enzyme Catalysis on the Size of the QM Region. *J Phys Chem B* **2016**, *120* (37), 9913-9921.
6. Casalino, L.; Palermo, G.; Rothlisberger, U.; Magistrato, A., Who Activates the Nucleophile in Ribozyme Catalysis? An Answer from the Splicing Mechanism of Group II Introns. *Journal of the American Chemical Society* **2016**, *138* (33), 10374-10377.
7. Cortopassi, W. A.; Kumar, K.; Duarte, F.; Pimentel, A. S.; Paton, R. S., Mechanisms of Histone Lysine-modifying Enzymes: A Computational Perspective on the Role of the Protein Environment. *Journal of Molecular Graphics & Modelling* **2016**, *67*, 69-84.
8. Gillet, N.; Ruiz-Pernia, J. J.; de la Lande, A.; Levy, B.; Lederer, F.; Demachy, I.; Moliner, V., QM/MM study of L-lactate Oxidation by Flavocytochrome b(2). *Physical Chemistry Chemical Physics* **2016**, *18* (23), 15609-15618.
9. Roston, D.; Demapan, D.; Cui, Q., Leaving Group Ability Observably Affects Transition State Structure in a Single Enzyme Active Site. *Journal of the American Chemical Society* **2016**, *138* (23), 7386-7394.
10. Samudio, B. M.; Couch, V.; Stuchebrukhov, A. A., Monte Carlo Simulations of Glu-242 in Cytochrome c Oxidase. *J Phys Chem B* **2016**, *120* (9), 2095-2105.
11. Ferrara, P.; Apostolakis, J.; Caflisch, A., Thermodynamics and Kinetics of Folding of Two Model Peptides Investigated by Molecular Dynamics Simulations. *The Journal of Physical Chemistry B* **2000**, *104* (20), 5000-5010.
12. Leopold, P. E.; Montal, M.; Onuchic, J. N., Protein Folding Funnels: A Kinetic Approach to the Sequence-Structure Relationship. *Proceedings of the National Academy of Sciences* **1992**, *89* (18), 8721-8725.
13. Onuchic, J. N.; Socci, N. D.; Luthey-Schulten, Z.; Wolynes, P. G., Protein Folding Funnels: The Nature of the Transition State Ensemble. *Folding and Design* **1996**, *1* (6), 441-450.
14. Šali, A.; Shakhnovich, E.; Karplus, M., How Does a Protein Fold? *Nature* **1994**, *369* (6477), 248-251.
15. Šali, A.; Shakhnovich, E.; Karplus, M., Kinetics of Protein Folding. *Journal of Molecular Biology* **1994**, *235* (5), 1614-1636.

- 1
2
3
4
5
6
7
8
9
10
11
12
13
14
15
16
17
18
19
20
21
22
23
24
25
26
27
28
29
30
31
32
33
34
35
36
37
38
39
40
41
42
43
44
45
46
47
48
49
50
51
52
53
54
55
56
57
58
59
60
16. Snow, C. D.; Nguyen, N.; Pande, V. S.; Gruebele, M., Absolute Comparison of Simulated and Experimental Protein-folding Dynamics. *Nature* **2002**, *420* (6911), 102-106.
 17. Dill, K. A.; Ozkan, S. B.; Shell, M. S.; Weikl, T. R., The Protein Folding Problem. In *Annual Review of Biophysics*, 2008; Vol. 37, pp 289-316.
 18. Shea, J. E.; Brooks, C. L., From Folding Theories to Folding Proteins: A Review and Assessment of Simulation Studies of Protein Folding and Unfolding. *Annual Review of Physical Chemistry* **2001**, *52*, 499-535.
 19. Gallicchio, E.; Levy, R. M., Recent Theoretical and Computational Advances for Modeling Protein-Ligand Binding Affinities. In *Computational chemistry methods in structural biology*, Elsevier BV: 2011; pp 27-80.
 20. Jorgensen, W. L., The Many Roles of Computation in Drug Discovery. *Science* **2004**, *303* (5665), 1813-1818.
 21. Marelus, J.; Hansson, T.; Åqvist, J., Calculation of Ligand Binding Free Energies from Molecular Dynamics Simulations. *Int. J. Quant. Chem.* **1998**, *69* (1), 77-88.
 22. Wereszczynski, J.; McCammon, J. A., Statistical Mechanics and Molecular Dynamics in Evaluating Thermodynamic Properties of Biomolecular Recognition. *Quarterly Reviews of Biophysics* **2011**, *45* (01), 1-25.
 23. Gilson, M. K.; Zhou, H. X., Calculation of Protein-Ligand Binding Affinities. In *Annual Review of Biophysics and Biomolecular Structure*, 2007; Vol. 36, pp 21-42.
 24. Grubmuller, H.; Heymann, B.; Tavan, P., Ligand Binding: Molecular Mechanics Calculation of the Streptavidin Biotin Rupture Force. *Science* **1996**, *271* (5251), 997-999.
 25. Isralewitz, B.; Gao, M.; Schulten, K., Steered Molecular Dynamics and Mechanical Functions of Proteins. *Current Opinion in Structural Biology* **2001**, *11* (2), 224-230.
 26. Sherman, W.; Day, T.; Jacobson, M. P.; Friesner, R. A.; Farid, R., Novel Procedure for Modeling Ligand/Receptor Induced Fit Effects. *Journal of Medicinal Chemistry* **2006**, *49* (2), 534-553.
 27. Böckmann, R. A.; Grubmüller, H., Nanoseconds Molecular Dynamics Simulation of Primary Mechanical Energy Transfer Steps in F1-ATP Synthase. *Nature Structural Biology* **2002**, *9* (198-202).
 28. Kruger, P., Extending the Capabilities of Targeted Molecular Dynamics: Simulation of a Large Conformational Transition in Plasminogen Activator Inhibitor 1. *Protein Science* **2001**, *10* (4), 798-808.
 29. Ma, J.; Sigler, P. B.; Xu, Z.; Karplus, M., A Dynamic Model for the Allosteric Mechanism of GroEL. *Journal of Molecular Biology* **2000**, *302* (2), 303-313.
 30. Yang, W.; Gao, Y. Q.; Cui, Q.; Ma, J.; Karplus, M., The Missing Link Between Thermodynamics and Structure in F1-ATPase. *Proceedings of the National Academy of Sciences* **2003**, *100* (3), 874-879.
 31. Shukla, D.; Meng, Y. L.; Roux, B.; Pande, V. S., Activation Pathway of Src Kinase Reveals Intermediate States as Targets for Drug Design. *Nature Communications* **2014**, *5*, 3397.
 32. Onufriev, A.; Bashford, D.; Case, D. A., Exploring Protein Native States and Large-scale Conformational Changes with a Modified Generalized Born Model. *Proteins-Structure Function and Bioinformatics* **2004**, *55* (2), 383-394.
 33. Splettstoesser, T.; Holmes, K. C.; Noe, F.; Smith, J. C., Structural Modeling and Molecular Dynamics Simulation of the Actin Filament. *Proteins-Structure Function and Bioinformatics* **2011**, *79* (7), 2033-2043.

- 1
2
3 34. Kulik, H. J.; Luehr, N.; Ufimtsev, I. S.; Martinez, T. J., Ab Initio Quantum Chemistry for
4 Protein Structures. *The Journal of Physical Chemistry B* **2012**, *116* (41), 12501-12509.
- 5 35. Rudberg, E.; Rubensson, E. H.; Safek, P., Hartree–Fock Calculations with Linearly
6 Scaling Memory Usage. *The Journal of Chemical Physics* **2008**, *128* (18), 184106.
- 7 36. Ufimtsev, I. S.; Luehr, N.; Martinez, T. J., Charge Transfer and Polarization in Solvated
8 Proteins from Ab Initio Molecular Dynamics. *J. Phys. Chem. Lett.* **2011**, *2* (14), 1789-1793.
- 9 37. Lifson, S., Consistent Force Field for Calculations of Conformations, Vibrational Spectra,
10 and Enthalpies of Cycloalkane and n-Alkane Molecules. *The Journal of Chemical Physics* **1968**,
11 *49* (11), 5116.
- 12 38. Levitt, M.; Lifson, S., Refinement of Protein Conformations using a Macromolecular
13 Energy Minimization Procedure. *Journal of Molecular Biology* **1969**, *46* (2), 269-279.
- 14 39. Jorgensen, W. L.; Tirado-Rives, J., The OPLS [Optimized Potentials for Liquid
15 Simulations] Potential Functions for Proteins, Energy Minimizations for Crystals of Cyclic
16 Peptides and Crambin. *Journal of the American Chemical Society* **1988**, *110* (6), 1657-1666.
- 17 40. Brooks, B. R.; Bruccoleri, R. E.; Olafson, B. D.; States, D. J.; Swaminathan, S.; Karplus,
18 M., Charmm - A Program For Macromolecular Energy, Minimization, And Dynamics
19 Calculations. *Journal of Computational Chemistry* **1983**, *4* (2), 187-217.
- 20 41. MacKerell, A. D.; Bashford, D.; Bellott, M.; Dunbrack, R. L.; Evanseck, J. D.; Field, M.
21 J.; Fischer, S.; Gao, J.; Guo, H.; Ha, S.; et al., All-atom Empirical Potential for Molecular
22 Modeling and Dynamics Studies of Proteins. *J Phys Chem B* **1998**, *102* (18), 3586-3616.
- 23 42. Mackerell, A. D.; Feig, M.; Brooks, C. L., Extending the Treatment of Backbone
24 Energetics in Protein Force Fields: Limitations of Gas-Phase Quantum Mechanics in
25 Reproducing Protein Conformational Distributions in Molecular Dynamics Simulations. *Journal*
26 *of Computational Chemistry* **2004**, *25* (11), 1400-1415.
- 27 43. Huang, J.; MacKerell, A. D., CHARMM36 All-Atom Additive Protein Force Field:
28 Validation Based on Comparison to NMR Data. *Journal of Computational Chemistry* **2013**, *34*
29 (25), 2135-2145.
- 30 44. Lopes, P. E. M.; Guvench, O.; MacKerell, A. D., Current Status of Protein Force Fields
31 for Molecular Dynamics Simulations. In *Molecular Modeling of Proteins: 2nd Edition*, Kukol,
32 A., Ed. 2015; Vol. 1215, pp 47-71.
- 33 45. Ponder, J. W.; Case, D. A., Force Fields for Protein Simulations. *Protein Simulations*
34 **2003**, *66*, 27-85.
- 35 46. Mackerell, A. D., Empirical Force Fields for Biological Macromolecules: Overview and
36 Issues. *Journal of Computational Chemistry* **2004**, *25* (13), 1584-1604.
- 37 47. Wang, W.; Donini, O.; Reyes, C. M.; Kollman, P. A., Biomolecular Simulations: Recent
38 Developments in Force Fields, Simulations of Enzyme Catalysis, Protein-Ligand, Protein-Protein,
39 and Protein-Nucleic Acid Noncovalent Interactions. *Annual Review of Biophysics and*
40 *Biomolecular Structure* **2001**, *30*, 211-243.
- 41 48. Cornell, W. D.; Cieplak, P.; Bayly, C. I.; Gould, I. R.; Merz, K. M.; Ferguson, D. M.;
42 Spellmeyer, D. C.; Fox, T.; Caldwell, J. W.; Kollman, P. A., A Second Generation Force Field
43 for the Simulation of Proteins, Nucleic Acids, and Organic Molecules. *J. Am. Chem. Soc.* **1995**,
44 *117* (19), 5179-5197.
- 45 49. Bayly, C. I.; Cieplak, P.; Cornell, W.; Kollman, P. A., A Well-behaved Electrostatic
46 Potential Based Method using Charge Restraints for Deriving Atomic Charges: The RESP Model.
47 *The Journal of Physical Chemistry* **1993**, *97* (40), 10269-10280.
- 48
49
50
51
52
53
54
55
56
57
58
59
60

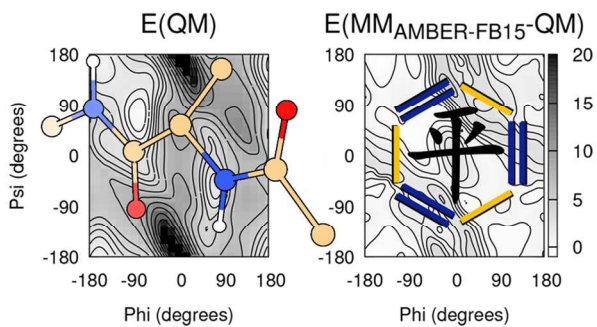
- 1
2
3 50. Jakalian, A.; Bush, B. L.; Jack, D. B.; Bayly, C. I., Fast, Efficient Generation of High-
4 Quality Atomic Charges. AM1-BCC model: I. Method. *Journal of Computational Chemistry*
5 **2000**, *21* (2), 132-146.
- 6
7 51. Jakalian, A.; Jack, D. B.; Bayly, C. I., Fast, Efficient Generation of High-Quality Atomic
8 Charges. AM1-BCC model: II. Parameterization and Validation. *Journal of Computational*
9 *Chemistry* **2002**, *23* (16), 1623-1641.
- 10 52. Wang, J.; Cieplak, P.; Kollman, P. A., How Well Does a Restrained Electrostatic
11 Potential (RESP) Model Perform in Calculating Conformational Energies of Organic and
12 Biological Molecules? *Journal of Computational Chemistry* **2000**, *21* (12), 1049-1074.
- 13 53. Hornak, V.; Abel, R.; Okur, A.; Strockbine, B.; Roitberg, A.; Simmerling, C.,
14 Comparison of Multiple Amber Force Fields and Development of Improved Protein Backbone
15 Parameters. *Proteins: Structure, Function, and Bioinformatics* **2006**, *65* (3), 712-725.
- 16 54. Garcia, A. E.; Sanbonmatsu, K. Y., Helical Stabilization by Side Chain Shielding of
17 Backbone Hydrogen Bonds. *Proceedings of the National Academy of Sciences* **2002**, *99* (5),
18 2782-2787.
- 19
20 55. Lindorff-Larsen, K.; Piana, S.; Palmo, K.; Maragakis, P.; Klepeis, J. L.; Dror, R. O.;
21 Shaw, D. E., Improved Side-Chain Torsion Potentials for the Amber ff99SB Protein Force Field.
22 *Proteins: Structure, Function, and Bioinformatics* **2010**, *78* (8), 1950-1958.
- 23 56. Feyereisen, M.; Fitzgerald, G.; Komornicki, A., Use Of Approximate Integrals In
24 Abinitio Theory - An Application In MP2 Energy Calculations. *Chemical Physics Letters* **1993**,
25 *208* (5-6), 359-363.
- 26 57. Distasio, R. A.; Steele, R. P.; Rhee, Y. M.; Shao, Y. H.; Head-Gordon, M., An Improved
27 Algorithm for Analytical Gradient Evaluation in Resolution-of-the-Identity Second-Order
28 Moller-Plesset Perturbation Theory: Application to Alanine Tetrapeptide Conformational
29 Analysis. *Journal of Computational Chemistry* **2007**, *28* (5), 839-856.
- 30 58. Kendall, R. A.; Dunning, T. H.; Harrison, R. J., Electron-Affinities Of The 1st-Row
31 Atoms Revisited - Systematic Basis-Sets And Wave-Functions. *J Chem Phys* **1992**, *96* (9), 6796-
32 6806.
- 33 59. Li, D. W.; Bruschiweiler, R., NMR-Based Protein Potentials. *Angewandte Chemie-*
34 *International Edition* **2010**, *49* (38), 6778-6780.
- 35 60. Shaw, D. E.; Maragakis, P.; Lindorff-Larsen, K.; Piana, S.; Dror, R. O.; Eastwood, M. P.;
36 Bank, J. A.; Jumper, J. M.; Salmon, J. K.; Shan, Y.; Wriggers, W., Atomic-Level
37 Characterization of the Structural Dynamics of Proteins. *Science* **2010**, *330* (6002), 341-346.
- 38 61. Cerutti, D. S.; Rice, J. E.; Swope, W. C.; Case, D. A., Derivation of Fixed Partial Charges
39 for Amino Acids Accommodating a Specific Water Model and Implicit Polarization. *J Phys*
40 *Chem B* **2013**, *117* (8), 2328-2338.
- 41 62. Debiec, K. T.; Cerutti, D. S.; Baker, L. R.; Gronenborn, A. M.; Case, D. A.; Chong, L. T.,
42 Further along the Road Less Traveled: AMBER ff15ipq, an Original Protein Force Field Built on
43 a Self-Consistent Physical Model. *J. Chem. Theory Comput.* **2016**, *12* (8), 3926-3947.
- 44 63. Lopes, P. E. M.; Huang, J.; Shim, J.; Luo, Y.; Li, H.; Roux, B.; MacKerell, A. D.,
45 Polarizable Force Field for Peptides and Proteins Based on the Classical Drude Oscillator. *J.*
46 *Chem. Theory Comput.* **2013**, *9* (12), 5430-5449.
- 47 64. Shi, Y.; Xia, Z.; Zhang, J.; Best, R.; Wu, C.; Ponder, J. W.; Ren, P., Polarizable Atomic
48 Multipole-Based AMOEBA Force Field for Proteins. *J. Chem. Theory Comput.* **2013**, *9* (9),
49 4046-4063.
- 50
51
52
53
54
55
56
57
58
59
60

- 1
2
3
4
5
6
7
8
9
10
11
12
13
14
15
16
17
18
19
20
21
22
23
24
25
26
27
28
29
30
31
32
33
34
35
36
37
38
39
40
41
42
43
44
45
46
47
48
49
50
51
52
53
54
55
56
57
58
59
60
65. Wang, L.-P.; Martinez, T. J.; Pande, V. S., Building Force Fields: An Automatic, Systematic, and Reproducible Approach. *J. Phys. Chem. Lett.* **2014**, *5* (11), 1885-1891.
66. Horn, H. W.; Swope, W. C.; Pitera, J. W.; Madura, J. D.; Dick, T. J.; Hura, G. L.; Head-Gordon, T., Development of an Improved Four-Site Water Model for Biomolecular Simulations: TIP4P-Ew. *J Chem Phys* **2004**, *120* (20), 9665-9678.
67. Darden, T.; York, D.; Pedersen, L., Particle Mesh Ewald - An N.Log(N) Method For Ewald Sums In Large Systems. *J Chem Phys* **1993**, *98* (12), 10089-10092.
68. Wang, L.-P. ForceBalance code and data repository on GitHub. <https://github.com/leeping/forcebalance> (accessed 2016/11/03).
69. Helgaker, T.; Klopper, W.; Koch, H.; Noga, J., Basis-Set Convergence of Correlated Calculations on Water. *J Chem Phys* **1997**, *106* (23), 9639-9646.
70. Merrick, J. P.; Moran, D.; Radom, L., An Evaluation of Harmonic Vibrational Frequency Scale Factors. *Journal of Physical Chemistry A* **2007**, *111* (45), 11683-11700.
71. Wang, L.-P.; Chen, J.; Van Voorhis, T., Systematic Parametrization of Polarizable Force Fields from Quantum Chemistry Data. *J. Chem. Theory Comput.* **2013**, *9* (1), 452-460.
72. Wang, L.-P.; Head-Gordon, T.; Ponder, J. W.; Ren, P.; Chodera, J. D.; Eastman, P. K.; Martinez, T. J.; Pande, V. S., Systematic Improvement of a Classical Molecular Model of Water. *The Journal of Physical Chemistry B* **2013**, *117* (34), 9956-9972.
73. Zhou, C. Y.; Jiang, F.; Wu, Y. D., Residue-Specific Force Field Based on Protein Coil Library. RSFF2: Modification of AMBER ff99SB. *J Phys Chem B* **2015**, *119* (3), 1035-1047.
74. Maier, J. A.; Martinez, C.; Kasavajhala, K.; Wickstrom, L.; Hauser, K. E.; Simmerling, C., ff14SB: Improving the Accuracy of Protein Side Chain and Backbone Parameters from ff99SB. *Journal of Chemical Theory and Computation* **2015**, *11* (8), 3696-3713.
75. Dennis, J. E.; Gay, D. M.; Walsh, R. E., An Adaptive Nonlinear Least-Squares Algorithm. *ACM Transactions on Mathematical Software* **1981**, *7* (3), 348-368.
76. Marquardt, D. W., An Algorithm for Least-Squares Estimation of Nonlinear Parameters. *Journal of the Society for Industrial and Applied Mathematics* **1963**, *11* (2), 431-441.
77. Moré, J. J., The Levenberg-Marquardt Algorithm: Implementation and Theory. In *Lecture Notes in Mathematics*, Springer Nature: 1978; pp 105-116.
78. Moré, J. J.; Sorensen, D. C., Computing a Trust Region Step. *SIAM Journal on Scientific and Statistical Computing* **1983**, *4* (3), 553-572.
79. Jones, E.; Oliphant, T.; Peterson, P.; others SciPy: Open Source Scientific Tools for Python. <http://www.scipy.org/> (accessed 2016/11/11).
80. Ponder, J. W. TINKER: Software Tools for Molecular Design. (accessed 2016/10/22).
81. Krylov, A. I.; Gill, P. M. W., Q-Chem: an engine for innovation. *Wiley Interdisciplinary Reviews: Computational Molecular Science* **2012**, *3* (3), 317-326.
82. Shao, Y.; Gan, Z.; Epifanovsky, E.; Gilbert, A. T. B.; Wormit, M.; Kussmann, J.; Lange, A. W.; Behn, A.; Deng, J.; Feng, X.; et al., Advances in Molecular Quantum Chemistry Contained in the Q-Chem 4 Program Package. *Molecular Physics* **2015**, *113* (2), 184-215.
83. Albrecht, M.; Rajan, D.; Thain, D., Making Work Queue Cluster-Friendly for Data Intensive Scientific Applications. In *2013 IEEE International Conference on Cluster Computing (CLUSTER)*, Institute of Electrical and Electronics Engineers (IEEE): 2013.
84. Turney, J. M.; Simmonett, A. C.; Parrish, R. M.; Hohenstein, E. G.; Evangelista, F. A.; Fermann, J. T.; Mintz, B. J.; Burns, L. A.; Wilke, J. J.; Abrams, M. L.; et al., Psi4: An Open-Source Ab Initio Electronic Structure Program. *Wiley Interdisciplinary Reviews: Computational Molecular Science* **2011**, *2* (4), 556-565.

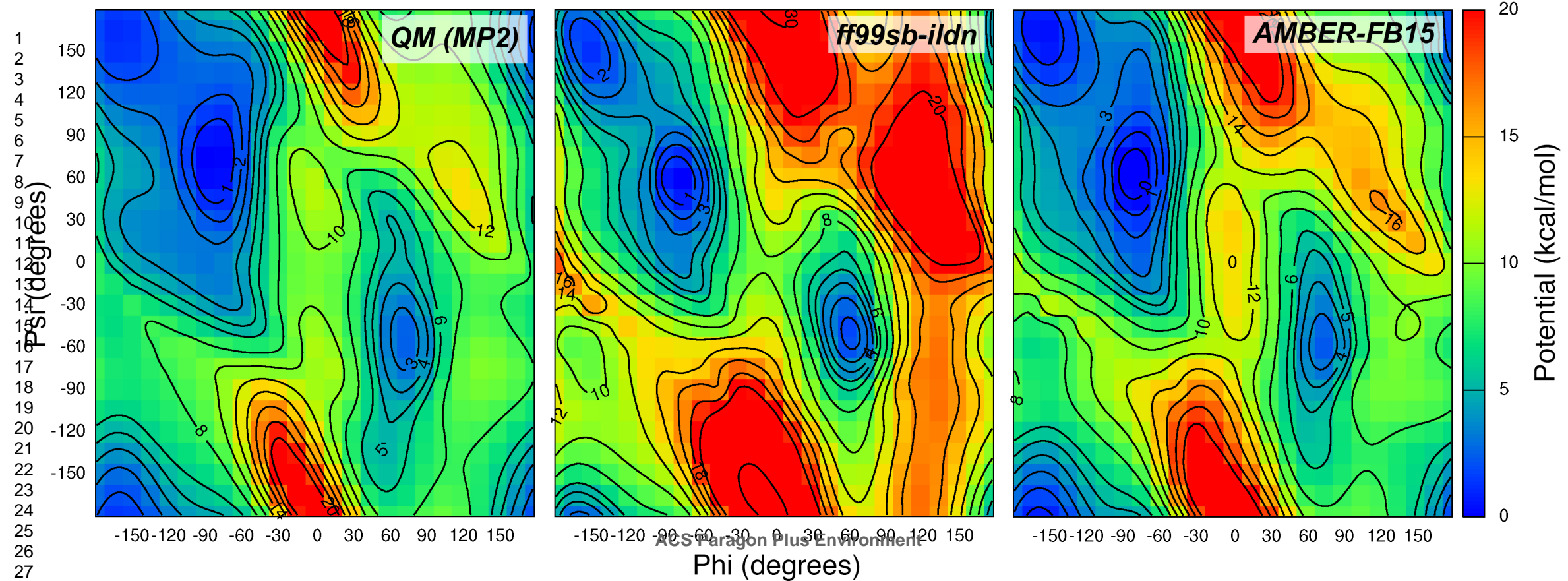
- 1
2
3
4
5
6
7
8
9
10
11
12
13
14
15
16
17
18
19
20
21
22
23
24
25
26
27
28
29
30
31
32
33
34
35
36
37
38
39
40
41
42
43
44
45
46
47
48
49
50
51
52
53
54
55
56
57
58
59
60
85. Abraham, M. J.; Murtola, T.; Schulz, R.; Páll, S.; Smith, J. C.; Hess, B.; Lindahl, E., GROMACS: High Performance Molecular Simulations through Multi-Level Parallelism from Laptops to Supercomputers. *SoftwareX* **2015**, *1-2*, 19-25.
86. McGibbon, R.T.; Beauchamp, K.A.; Harrigan, M.P.; Klein, C.; Swails, Jason M.; Hernández, C.X.; Schwantes, C.R.; Wang, L.-P.; Lane, T.J.; Pande, V.S., MDTraj: A Modern Open Library for the Analysis of Molecular Dynamics Trajectories. *Biophysical Journal* **2015**, *109* (8), 1528-1532.
87. Han, B.; Liu, Y. F.; Ginzinger, S. W.; Wishart, D. S., SHIFTX2: Significantly Improved Protein Chemical Shift Prediction. *Journal of Biomolecular Nmr* **2011**, *50* (1), 43-57.
88. Swails, J. M.; Hernandez, C. X.; Mobley, D. L.; Nguyen, H.; Wang, L.-P.; Janowski, P. ParmEd: Cross-Program Parameter and Topology File Editor and Molecular Mechanical Simulator Engine. <https://github.com/ParmEd/ParmEd> (accessed 2016/11/11).
89. Salomon-Ferrer, R.; Case, D. A.; Walker, R. C., An Overview of the Amber Biomolecular Simulation Package. *Wiley Interdisciplinary Reviews-Computational Molecular Science* **2013**, *3* (2), 198-210.
90. Roe, D. R.; Cheatham, T. E., PTRAJ and CPPTRAJ: Software for Processing and Analysis of Molecular Dynamics Trajectory Data. *Journal of Chemical Theory and Computation* **2013**, *9* (7), 3084-3095.
91. McGibbon, R. T.; Beauchamp, K. A.; Harrigan, M. P.; Klein, C.; Swails, J. M.; Hernandez, C. X.; Schwantes, C. R.; Wang, L. P.; Lane, T. J.; Pande, V. S., MDTraj: A Modern Open Library for the Analysis of Molecular Dynamics Trajectories. *Biophysical Journal* **2015**, *109* (8), 1528-1532.
92. Altunay, M.; Avery, P.; Blackburn, K.; Bockelman, B.; Ernst, M.; Fraser, D.; Quick, R.; Gardner, R.; Goasguen, S.; Levshina, T.; et al., A Science Driven Production Cyberinfrastructure-the Open Science Grid. *Journal of Grid Computing* **2011**, *9* (2), 201-218.
93. Aqvist, J., Ion Water Interaction Potentials Derived From Free-Energy Perturbation Simulations. *Journal of Physical Chemistry* **1990**, *94* (21), 8021-8024.
94. Anandakrishnan, R.; Aguilar, B.; Onufriev, A. V., H++3.0: Automating pK Prediction and the Preparation of Biomolecular Structures for Atomistic Molecular Modeling and Simulations. *Nucleic Acids Research* **2012**, *40* (W1), W537-W541.
95. Koller, A. N.; Schwalbe, H.; Gohlke, H., Starting Structure Dependence of NMR Order Parameters Derived from MD Simulations: Implications for Judging Force-Field Quality. *Biophysical Journal* **2008**, *95* (1), L4-L6.
96. Prompers, J. J.; Bruschweiler, R., General Framework for Studying the Dynamics of Folded and Nonfolded Proteins by NMR Relaxation Spectroscopy and MD Simulation. *Journal of the American Chemical Society* **2002**, *124* (16), 4522-4534.
97. Smith, L. J.; Bowen, A. M.; Di Paolo, A.; Matagne, A.; Redfield, C., The Dynamics of Lysozyme from Bacteriophage Lambda in Solution Probed by NMR and MD Simulations. *Chembiochem* **2013**, *14* (14), 1780-1788.
98. Smith, L. J.; van Gunsteren, W. F.; Hansen, N., Characterization of the Flexible Lip Regions in Bacteriophage Lambda Lysozyme using MD Simulations. *Eur. Biophys. J. Biophys. Lett.* **2015**, *44* (4), 235-247.
99. Case, D. A., Interpretation of Chemical Shifts and Coupling Constants in Macromolecules. *Current Opinion in Structural Biology* **2000**, *10* (2), 197-203.

- 1
2
3 100. Case, D. A.; Scheurer, C.; Bruschweiler, R., Static and dynamic effects on vicinal scalar J
4 couplings in proteins and peptides: A MD/DFT analysis. *Journal of the American Chemical*
5 *Society* **2000**, *122* (42), 10390-10397.
- 6
7 101. Perez, C.; Lohr, F.; Ruterjans, H.; Schmidt, J. M., Self-Consistent Karplus
8 Parametrization of (3)J Couplings Depending on the Polypeptide Side-Chain Torsion Chi(1).
9 *Journal of the American Chemical Society* **2001**, *123* (29), 7081-7093.
- 10
11 102. Schmidt, J. M.; Blumel, M.; Lohr, F.; Ruterjans, H., Self-Consistent (3)J Coupling
12 Analysis for the Joint Calibration of Karplus Coefficients and Evaluation of Torsion Angles.
13 *Journal of Biomolecular Nmr* **1999**, *14* (1), 1-12.
- 14
15 103. Vuister, G. W.; Bax, A., Quantitative J Correlation - A New Approach For Measuring
16 Homonuclear 3-Bond J(H(N)H(Alpha) Coupling-Constants In N-15-Enriched Proteins. *Journal*
17 *of the American Chemical Society* **1993**, *115* (17), 7772-7777.
- 18
19 104. Vuister, G. W.; Wang, A. C.; Bax, A., Measurement Of 3-Bond Nitrogen Carbon-J
20 Couplings In Proteins Uniformly Enriched In N-15 And C-13. *Journal of the American Chemical*
21 *Society* **1993**, *115* (12), 5334-5335.
- 22
23 105. Best, R. B.; Hummer, G., Optimized Molecular Dynamics Force Fields Applied to the
24 Helix-Coil Transition of Polypeptides. *J Phys Chem B* **2009**, *113* (26), 9004-9015.
- 25
26 106. Shalongo, W.; Dugad, L.; Stellwagen, E., Distribution Of Helicity Within The Model
27 Peptide Acetyl(AAQAA)(3)Amide. *Journal of the American Chemical Society* **1994**, *116* (18),
28 8288-8293.
- 29
30 107. Davis, C. M.; Xiao, S. F.; Raeigh, D. P.; Dyer, R. B., Raising the Speed Limit for beta-
31 Hairpin Formation. *Journal of the American Chemical Society* **2012**, *134* (35), 14476-14482.
- 32
33 108. Case, D. A.; Cheatham, T. E.; Darden, T.; Gohlke, H.; Luo, R.; Merz, K. M.; Onufriev,
34 A.; Simmerling, C.; Wang, B.; Woods, R. J., The Amber Biomolecular Simulation Programs.
35 *Journal of Computational Chemistry* **2005**, *26* (16), 1668-1688.
- 36
37 109. Pitera, J. W.; Swope, W., Understanding Folding and Design: Replica-Exchange
38 Simulations of "Trp-cage" Fly Mini-proteins. *P Natl Acad Sci USA* **2003**, *100* (13), 7587-7592.
- 39
40 110. Pang, Y.-P., FF12MC: A Revised AMBER Forcefield and New Protein Simulation
41 Protocol. *Proteins: Structure, Function, and Bioinformatics* **2016**, *84* (10), 1490-1516.
- 42
43 111. Harder, E.; Damm, W.; Maple, J.; Wu, C. J.; Reboul, M.; Xiang, J. Y.; Wang, L. L.;
44 Lupyan, D.; Dahlgren, M. K.; Knight, J. L.; et al., OPLS3: A Force Field Providing Broad
45 Coverage of Drug-like Small Molecules and Proteins. *Journal of Chemical Theory and*
46 *Computation* **2016**, *12* (1), 281-296.
- 47
48 112. Piana, S.; Lindorff-Larsen, K.; Shaw, D. E., How Robust Are Protein Folding
49 Simulations with Respect to Force Field Parameterization? *Biophysical Journal* **2011**, *100* (9),
50 L47-L49.
- 51
52 113. Lindorff-Larsen, K.; Maragakis, P.; Piana, S.; Eastwood, M. P.; Dror, R. O.; Shaw, D. E.,
53 Systematic Validation of Protein Force Fields against Experimental Data. *Plos One* **2012**, *7* (2),
54 e32131.
- 55
56 114. Nerenberg, P. S.; Head-Gordon, T., Optimizing Protein-Solvent Force Fields to
57 Reproduce Intrinsic Conformational Preferences of Model Peptides. *Journal of Chemical Theory*
58 *and Computation* **2011**, *7* (4), 1220-1230.
- 59
60 115. Nerenberg, P. S.; Jo, B.; So, C.; Tripathy, A.; Head-Gordon, T., Optimizing Solute-Water
van der Waals Interactions to Reproduce Solvation Free Energies. *J Phys Chem B* **2012**, *116*,
4524-4534.

- 1
2
3
4
5
6
7
8
9
10
11
12
13
14
15
16
17
18
19
20
21
22
23
24
25
26
27
28
29
30
31
32
33
34
35
36
37
38
39
40
41
42
43
44
45
46
47
48
49
50
51
52
53
54
55
56
57
58
59
60
116. Zhou, A. Q.; O'Hern, C. S.; Regan, L., Predicting the Side-Chain Dihedral Angle Distributions of Nonpolar, Aromatic, and Polar Amino Acids using Hard Sphere Models. *Proteins-Structure Function and Bioinformatics* **2014**, *82* (10), 2574-2584.
117. Lemkul, J. A.; Huang, J.; Roux, B.; MacKerell, A. D., An Empirical Polarizable Force Field Based on the Classical Drude Oscillator Model: Development History and Recent Applications. *Chemical Reviews* **2016**, *116* (9), 4983-5013.
118. Tompa, P., Unstructural Biology Coming of Age. *Current Opinion in Structural Biology* **2011**, *21* (3), 419-425.
119. Fawzi, N. L.; Phillips, A. H.; Ruscio, J. Z.; Doucleff, M.; Wemmer, D. E.; Head-Gordon, T., Structure and Dynamics of the Abeta(21-30) Peptide from the Interplay of NMR Experiments and Molecular Simulations. *J Am Chem Soc* **2008**, *130* (19), 6145-58.
120. Uversky, V. N.; Oldfield, C. J.; Dunker, A. K., Intrinsically Disordered Proteins in Human Diseases: Introducing the D(2) Concept. In *Annual Review of Biophysics*, 2008; Vol. 37, pp 215-246.
121. Skinner, J. J.; Yu, W.; Gichana, E. K.; Baxa, M. C.; Hinshaw, J. R.; Freed, K. F.; Sosnick, T. R., Benchmarking All-Atom Simulations using Hydrogen Exchange. *P Natl Acad Sci USA* **2014**, *111* (45), 15975-15980.
122. Lindorff-Larsen, K.; Trbovic, N.; Maragakis, P.; Piana, S.; Shaw, D. E., Structure and Dynamics of an Unfolded Protein Examined by Molecular Dynamics Simulation. *Journal of the American Chemical Society* **2012**, *134* (8), 3787-3791.
123. Piana, S.; Donchev, A. G.; Robustelli, P.; Shaw, D. E., Water Dispersion Interactions Strongly Influence Simulated Structural Properties of Disordered Protein States. *J Phys Chem B* **2015**, *119* (16), 5113-5123.
124. Henriques, J.; Skepo, M., Molecular Dynamics Simulations of Intrinsically Disordered Proteins: On the Accuracy of the TIP4P-D Water Model and the Representativeness of Protein Disorder Models. *Journal of Chemical Theory and Computation* **2016**, *12* (7), 3407-3415.



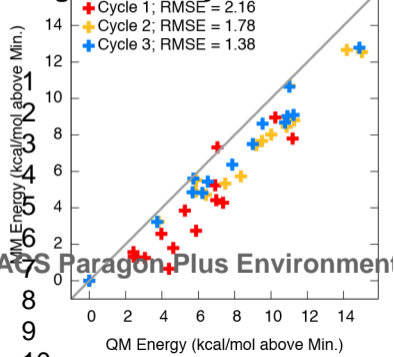
TOC graphic

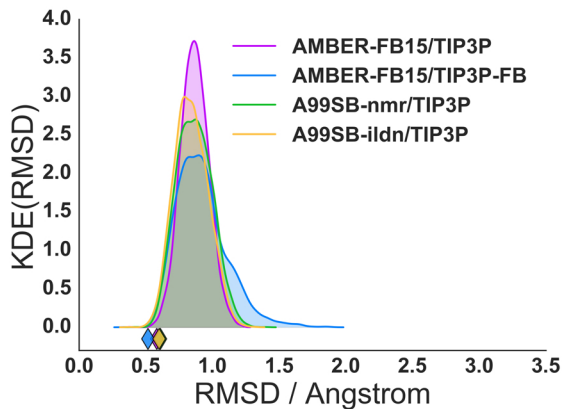
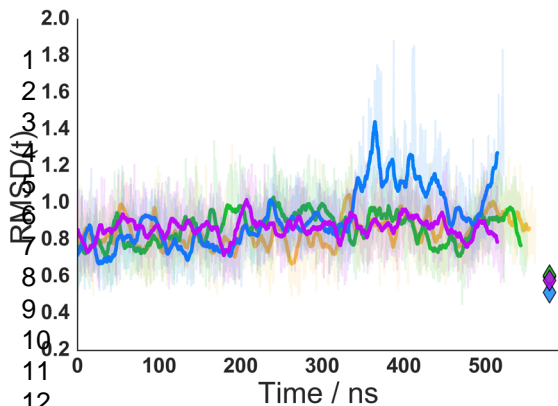


1
2
3
4
5
6
7
8
9
10
11
12
13
14
15
16
17
18
19
20
21
22
23
24
25
26
27
28

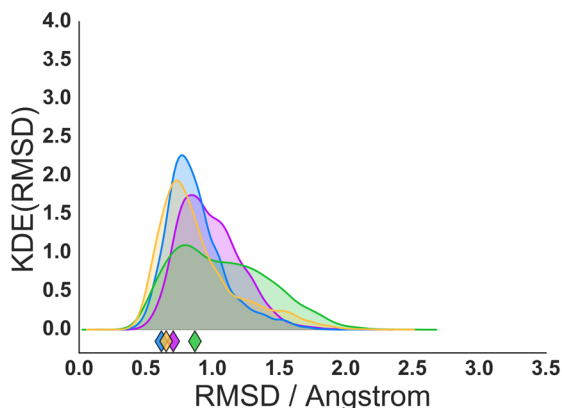
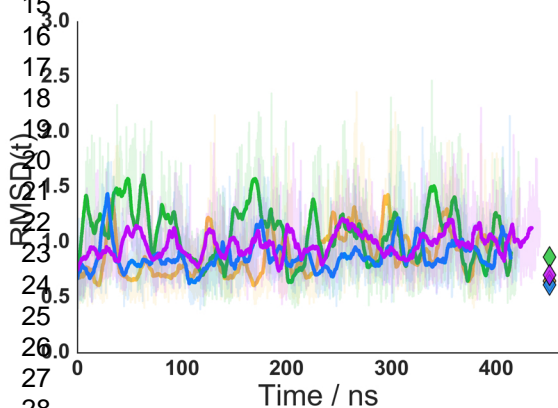
THR MM Optimized Structures

Page 49 of 54 Physical Chemistry

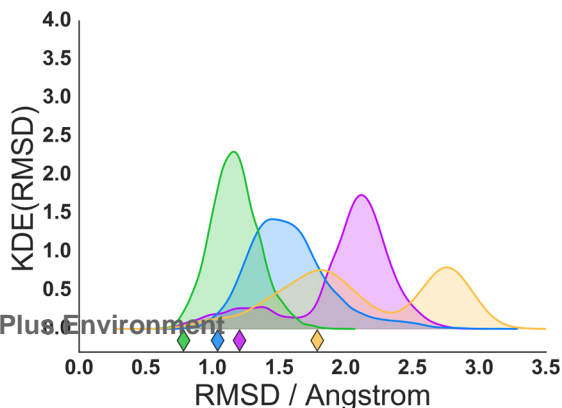
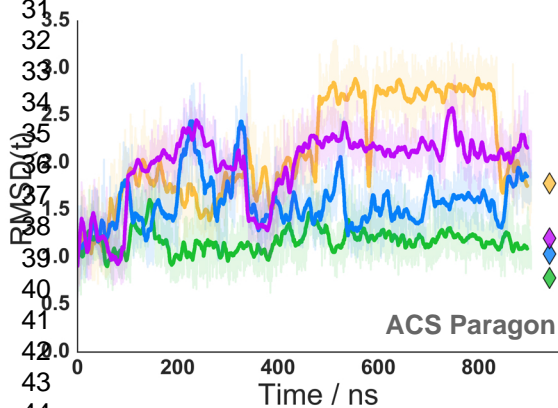




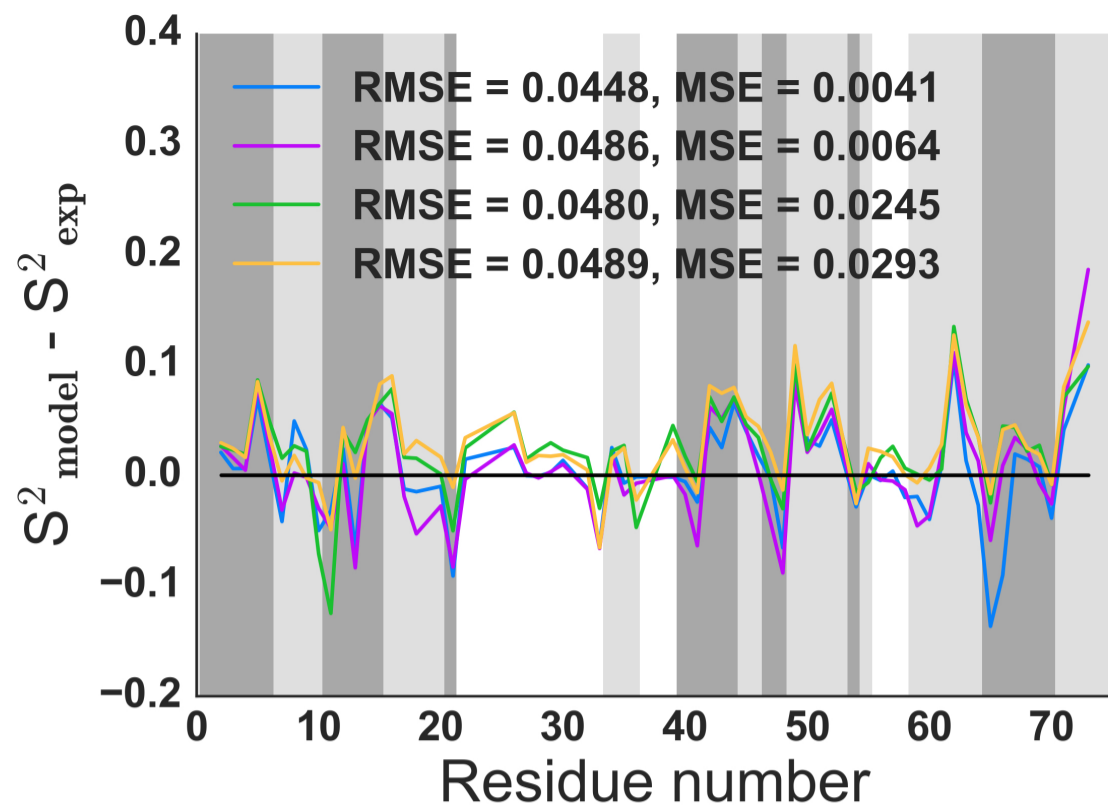
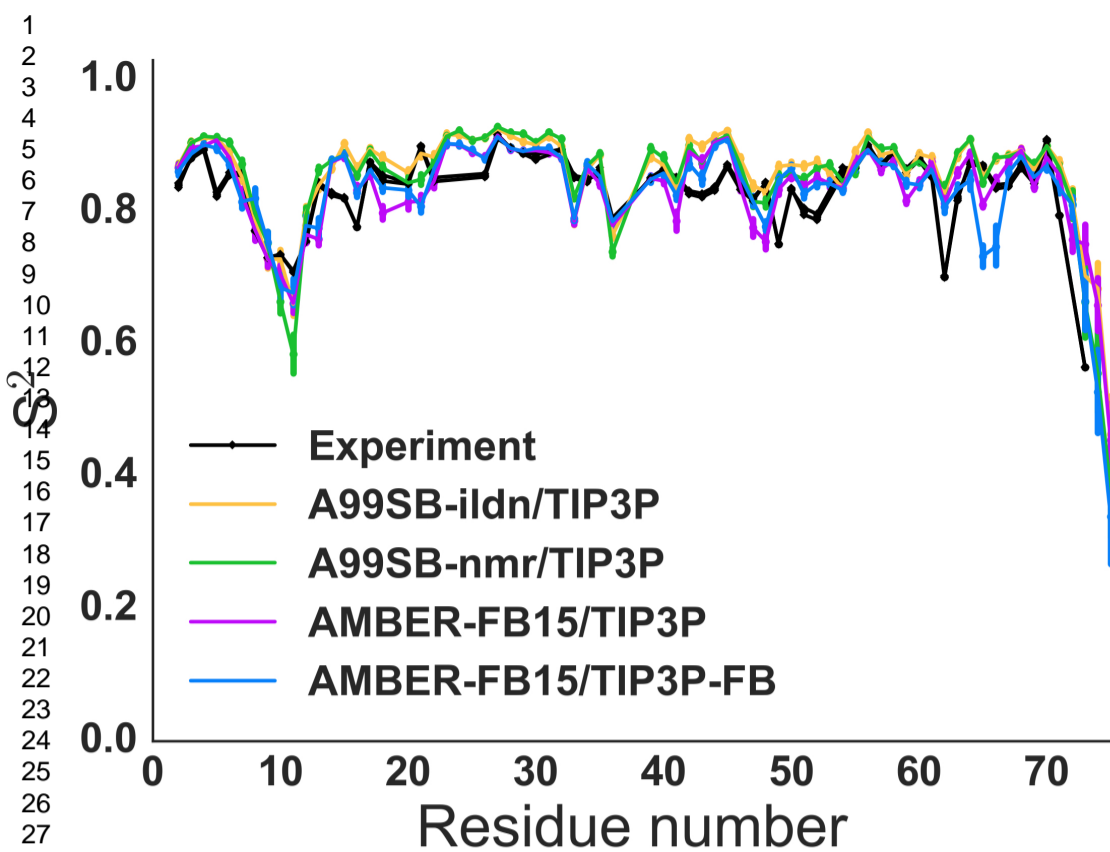
GB3



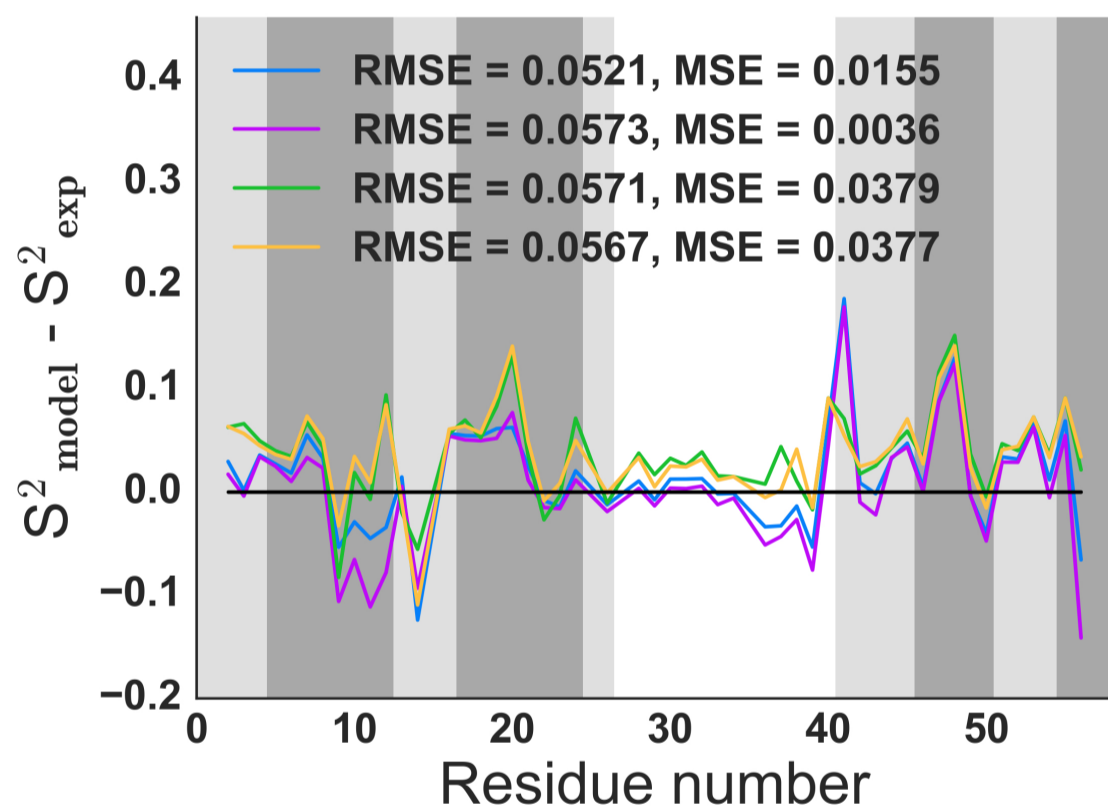
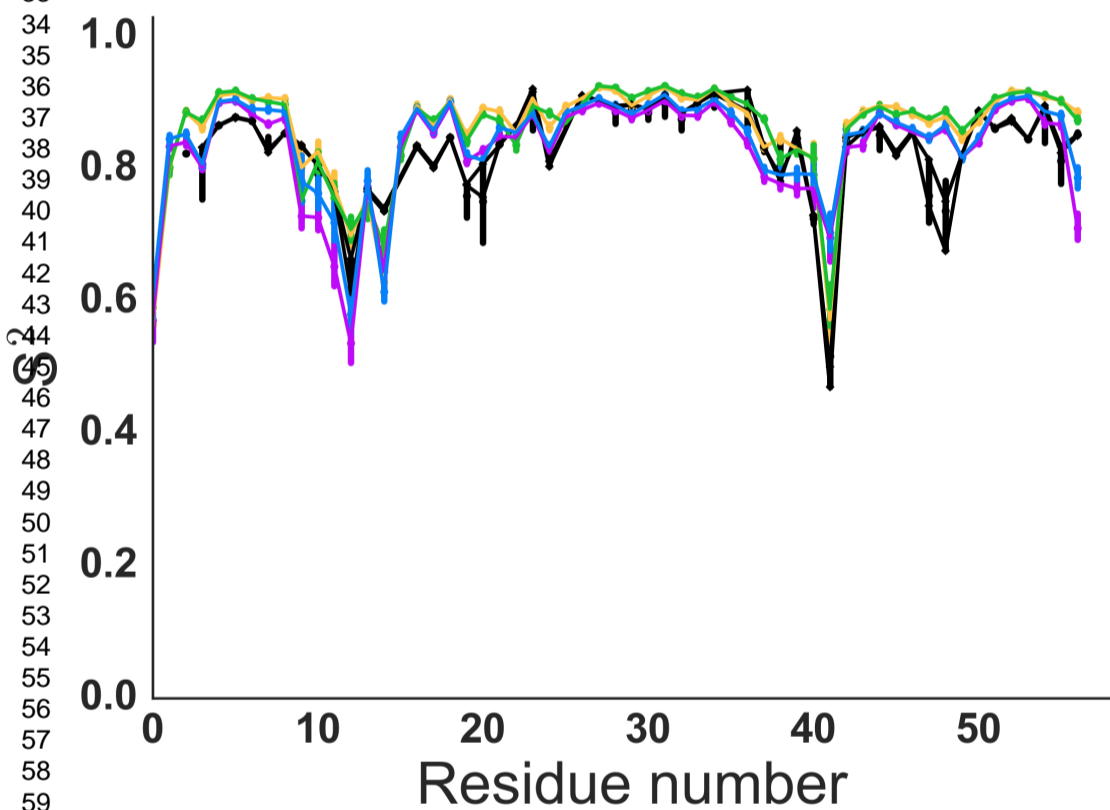
Lysozyme



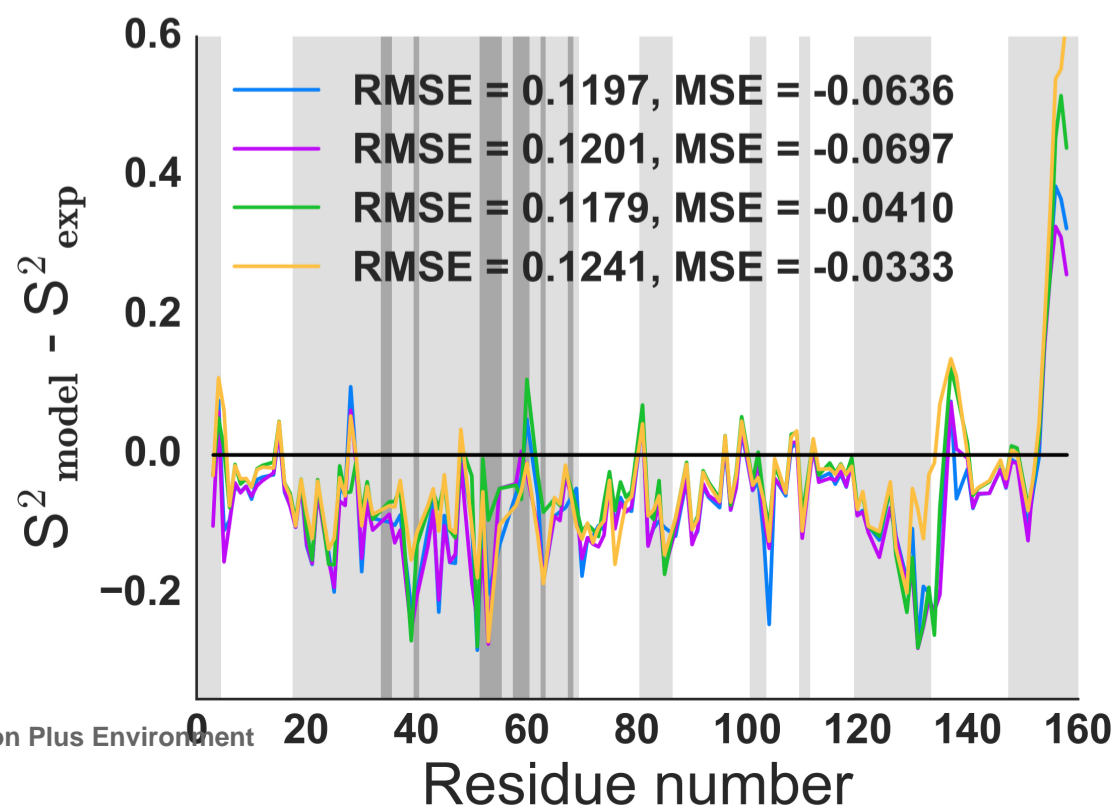
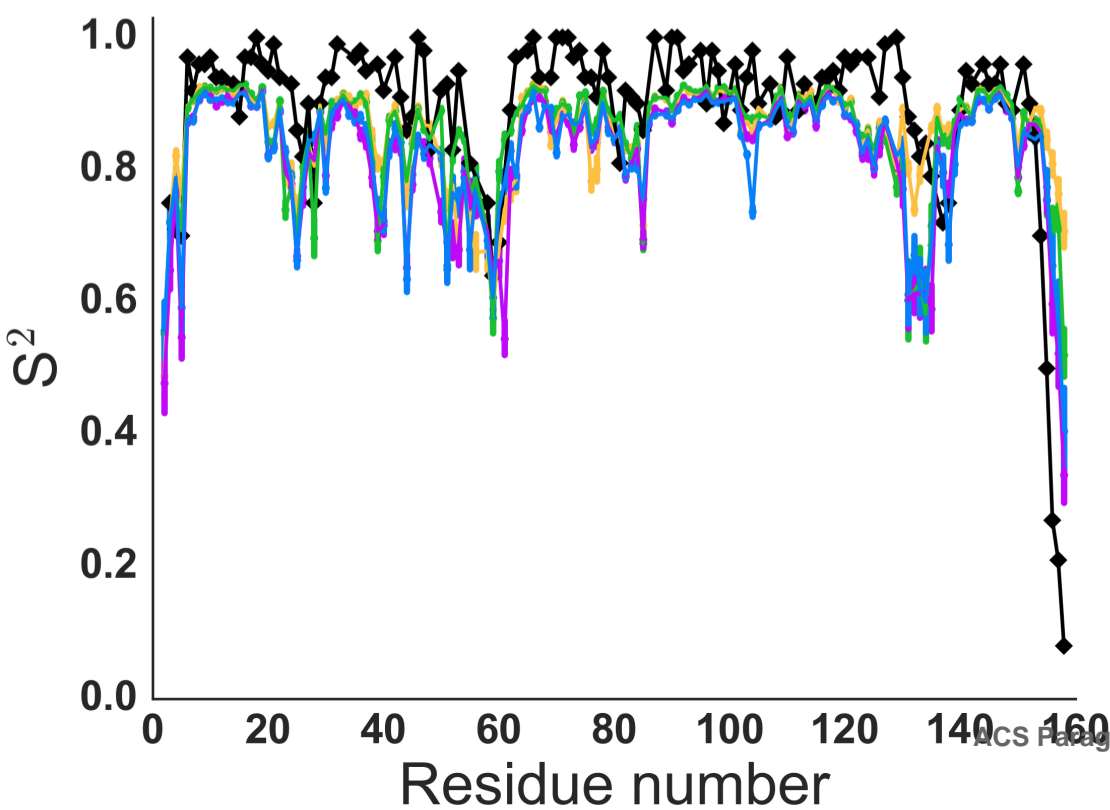
Ubiquitin



GB3



Lysozyme



Lysozyme Residue Number

GB3 Residue Number

